AD-A094 272 TEXAS A AND M UNIV COLLEGE STATION DEPT OF METEOROLOGY F/G 22/2
A COMPARATIVE ANALYSIS OF RAWINSONDE AND NIMBUS 6 AND TIROS N S--ETC(U)
JAN 81 J R SCOGGINS, W E CARLE, K KNIGHT DAAG29-76-G-0078
UNCLASSIFIED NASA-RP-1070 NL

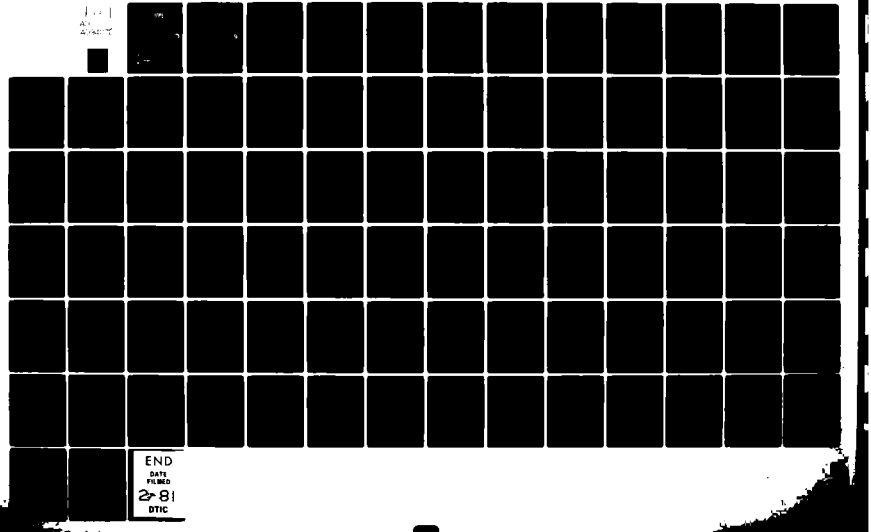

END
DATE FILMED
2-81
DTIC

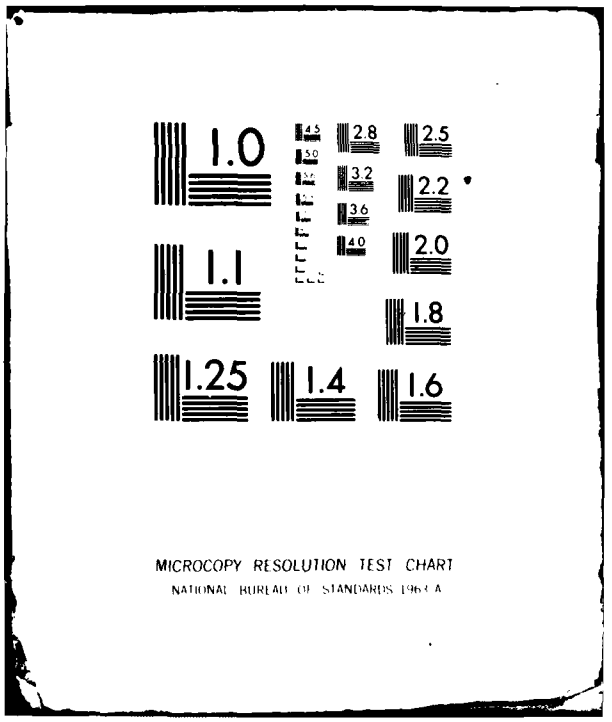
1.0
1.1
1.25
1.4
1.6
1.8
2.0
2.2
2.5
2.8
3.2
3.6
4.0
4.5
5.0
MICROCOPY RESOLUTION TEST CHART
NATIONAL BUREAU OF STANDARDS 1963 A

NASA Reference Publication 1070

A Comparative Analysis of Rawinsonde and Nimbus 6 and Tiros N Satellite Profile Data

James R. Scoggins, William E. Carle,
Keith Knight, Vance Moyer,
and Nine-Min Cheng

JANUARY 1981

NASA

NASA Reference Publication 1070

A Comparative Analysis of Rawinsonde and Nimbus 6 and Tiros N Satellite Profile Data

James R. Scoggins William E. Carle,
Keith Knight Vance Moyer,
and Nine-Min Cheng
Texas A&M University
College Station, Texas

NASA
National Aeronautics
and Space Administration

**Scientific and Technical
Information Branch**

1981

ACKNOWLEDGEMENTS

The authors express their sincere appreciation to Dr. William Smith and Mr. Harold Woolf of the National Environmental Satellite Service for providing the satellite data used in this study, Dr. Arthur Dodd of the Army Research Office for his interest and support while the study was in progress, and Dr. Gregory Wilson for performing the initial computations. Finally, the authors thank Mrs. Karen Hood for her assistance in preparing the final manuscript.

This research was supported by the U. S. Army Research Office, under Grant No. DAAG 29-76-G-0078 to the Department of Meteorology, Texas A&M University.

This report is published with the permission of the U.S. Army Research Office for use in connection with studies utilizing space technology for weather-related programs in progress in the Atmospheric Sciences Division, Space Sciences Laboratory, NASA, Marshall Space Flight Center.

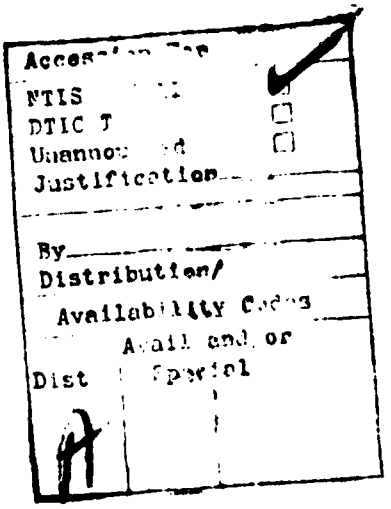

TABLE OF CONTENTS

TABLE OF CONTENTS (Continued)

TABLE OF CONTENTS (Continued)

LIST OF TABLES

LIST OF TABLES (Continued)

LIST OF FIGURES

LIST OF FIGURES (Continued)

LIST OF FIGURES (Continued)

LIST OF FIGURES (Continued)

A COMPARATIVE ANALYSIS OF RAWINSONDE AND NIMBUS-6 AND TIROS-N SATELLITE PROFILE DATA

James R. Scoggins, William E. Carle, Keith Knight,
Vance Moyer, and Nine-Min Cheng
Department of Meteorology, Texas A&M University

1. INTRODUCTION

1.1 Statement of the Problem

Rawinsonde data have traditionally been the principal source of upper air atmospheric data. Recently, however, satellites have become a major source of data and could allow improvement in our knowledge of the structure of the atmosphere because: 1) satellite soundings can be made on a global scale eliminating gaps in the data over the oceans; 2) all measurements would be made by the same instrument so that any errors resulting from the variability between rawinsonde instruments would be eliminated; and 3) the satellite measures the entire vertical extent of the sounding at one time so that errors resulting from the downstream drift of the balloon would be eliminated. However, before this new source of data may be fully utilized, studies must be done to determine the capabilities and limitations of satellite data for the purpose of determining atmospheric structure.

1.2 Previous Studies

The first vertical profiles of both temperature and water vapor were determined from measurements of two infrared spectrometers carried by the Nimbus-3 satellite. These data provided the first analysis of the three-dimensional thermodynamic structure of the atmosphere from satellite observations. The first studies (Wark and Hilleary, 1969; Hanel and Conrath, 1969) compared individual satellite temperature profiles with corresponding rawinsonde profiles; relatively good agreement was found.

Staelin et al. (1973) found temperature differences between Nimbus-5 and radiosonde profiles ranging between 1 and 4 K over an altitude range of 1 to 20 km, with the largest discrepancies found at the tropopause and near the surface. Layer-mean temperature differences between satellite

---

* Research supported by U. S. Army Research Office, Research Triangle Park, North Carolina, under Grant DAAG 29-76-G-0078 to the Department of Meteorology, Texas A&M University.

and radiosonde data for 13 pressure levels were found by Waters et al. (1975) to be 2.1 K in December and 1.6 K in June. Satellite-derived thicknesses were compared with rawinsonde layer thicknesses by Wilcox and Sanders (1976). Standard deviations of 45, 49, and 115 m for the layers 1000-500, 500-250, and 250-50 mb, respectively, were found.

Kapela and Horn (1975) compared isentropic cross sections from 1200 GMT radiosonde data with those from Nimbus-5 soundings, and found agreement with regard to patterns of isolines, but considerably less detail in the satellite cross section than in the radiosonde cross section. The same was true in cross sections of geostrophic and gradient wind.

Smith et al. (1975) used Nimbus-5 soundings to obtain geostrophic wind components perpendicular to cross sections in four separate case studies. Their satellite-derived geostrophic winds showed good correspondence with observed winds as well as geostrophic winds derived from radiosonde data. Arnold et al. (1976) compared cross sections of rawinsonde and Nimbus-5 temperatures and derived winds, and agreement was found as to general patterns but significant differences in cross sections of derived wind were present due to differences in horizontal temperature gradients obtained from the two types of data. Horn et al. (1976) compared cross sections of Nimbus-5 temperatures and derived winds from 1700 GMT satellite data with 1200 and 0000 GMT radiosonde data. They found the satellite patterns to be consistent with the changing synoptic situation, but with loss of detail.

In a study by Petersen and Horn (1977), temperature profiles obtained from Nimbus-6 radiance measurements were used along with sea-level pressures to construct gridded fields of 500-mb geopotential height and geostrophic wind over northeastern North America. Satellite-derived winds obtained at 1600 GMT were compared with geostrophic winds computed from 1200 and 0000 GMT rawinsonde height analyses. It was found that the isotach fields of geostrophic wind showed good continuity between satellite and bracketing rawinsonde analyses. Locations of the 500-mb velocity maximums were reasonably consistent between the two data sets. The rms differences between satellite and rawinsonde geostrophic wind fields ranged from 3.5 to 5.0 m s^{-1}.

Grody et al. (1979) considered the use of microwave radiometric measurements to infer atmospheric wind fields associated with tropical storms. In an analysis of Nimbus-6 data through typhoon June in November 1979, satellite-derived winds were compared with 700-mb aircraft reconnaissance winds. Major differences in wind speed occurred primarily near the storm center presumably because of the satellite sensor's insufficient horizontal resolution.

1.3 Objectives

The primary objective of this research is the determination of how well quantitative satellite data can be used to depict the structure of the atmosphere. This evaluation is made over a wide range of synoptic and surface conditions by comparing Nimbus-6 and TIROS-N data with rawinsonde data in several geographic regions. Satellite sounding data will be used to locate frontal zones and the tropopause, depict major features of the wind field, and determine the distribution of temperature gradients, moisture, and air mass stability. Atmospheric structure determined from satellite and rawinsonde data will be compared.

2. DATA UTILIZED

2.1 Satellite Data

Satellite data used in this study were provided by the National Environmental Satellite Service. Nimbus-6 data include temperature and dew-point temperature at 21 pressure levels (1000, 950, 920, 850, 780, 700, 670, 620, 570, 500, 475, 430, 400, 350, 300, 250, 200, 150, 135, 115, and 100 mb) at approximately 1700 GMT on 25 August 1975 and 0730 GMT on 3 September 1975. Nimbus-6 data for 1700 GMT on 5 February 1976 consist of only 10 reported levels (underlined above) and the data are of poorer quality than previous Nimbus-6 data because of deterioration of the High Resolution Infrared Radiation Sounder (HIRS). TIROS-N data include temperature and dew-point temperature at ten pressure levels (underlined above) at approximately 2100 GMT on 10 April 1979. Also included in the Nimbus-6 and TIROS-N data are the latitude, longitude, and the approximate surface elevation for each sounding.

2.2 Rawinsonde and Surface Data

Rawinsonde data for use in comparisons with Nimbus-6 data were obtained from the Texas A&M University archives of National Weather Service teletype data, and from the National Climatic Center. Quantities used include the temperature and dew-point temperature at mandatory and significant levels, and geopotential height and wind speed and direction at mandatory levels at 1200 GMT on 25 August 1975, 0000 GMT on 26 August 1975, 0000 and 1200 GMT on 3 September 1975, 1200 GMT on 5 February 1976, and 0000 GMT on 6 February 1976. As part of the AVE-SESAME project, rawinsonde soundings were taken at 2100 GMT on 10 April 1979. Twenty-one of these soundings have been processed at Texas A&M University for use in comparisons with TIROS-N sounding data. Surface hourly data used in the study include temperature, dew-point temperature, altimeter setting, and wind speed and direction at 1700 GMT on 25 August 1975, 0700 GMT on 3 September 1979, 1700 GMT on 5 February 1976, and 2100 GMT on 10 April 1979.

3. AREAS ANALYZED AND SYNOPTIC CONDITIONS

3.1 Areas Analyzed

Eight geographical areas representing a wide range of surface and synoptic conditions were chosen for analysis. The date, time, and location of these areas are listed in Table 1. These areas represent a variety of surface conditions including flat land, mountains, and water. Figure 1 shows the location of Areas I-IV and the distribution of rawinsonde and satellite data for each of these areas.

Table 1. List of areas chosen for analysis.

Area Number	Time/Date of Satellite Pass	Satellite Name	Area
I	1700 GMT, 25 August 1975	Nimbus-6	Central U.S.
II	1700 GMT, 25 August 1975	Nimbus-6	Caribbean
III	1700 GMT, 25 August 1975	Nimbus-6	Canada
IV	0730 GMT, 3 September 1975	Nimbus-6	Western U.S.
V	1700 GMT, 5 February 1976	Nimbus-6	Central U.S.
VI	1700 GMT, 5 February 1976	Nimbus-6	Caribbean
VII	1700 GMT, 5 February 1976	Nimbus-6	Canada
VIII	2100 GMT, 10 April 1979	TIROS-N	Central U.S.

3.2 Synoptic Conditions

The surface map at 1800 GMT on 25 August 1975 is shown in Fig. 2. A cold front extends from the Hudson Bay southwestward through the central United States. The occluded part of the cold front associated with a deep cyclone was located in the eastern part of Area III. The polar air was separated from the tropical air by the cold front extending through Area I, while Area II was covered entirely by an mT air mass. Horizontal gradients of pressure and temperature were large in Area III, moderate in Area I, and small in Area II.

Figure 3 shows the surface map in the vicinity of Area IV at 0600 GMT on 3 September 1975. The area was covered by a modified mP or cP air mass which was dry. Most of Area IV was free from convective activity with only a few thunderstorms in Arizona and New Mexico. Horizontal gradients of pressure and temperature were small in this area.

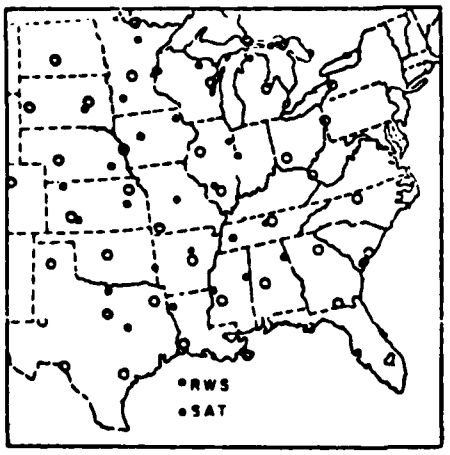

a. Area I

b. Area II

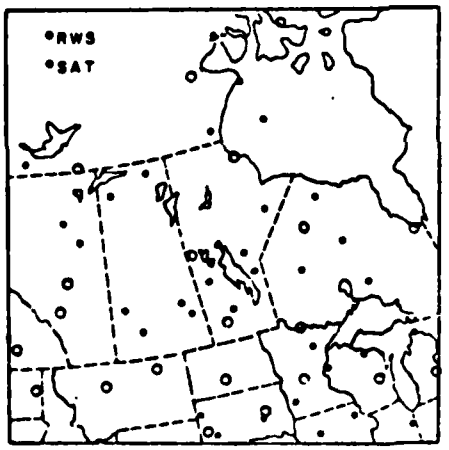

c. Area III

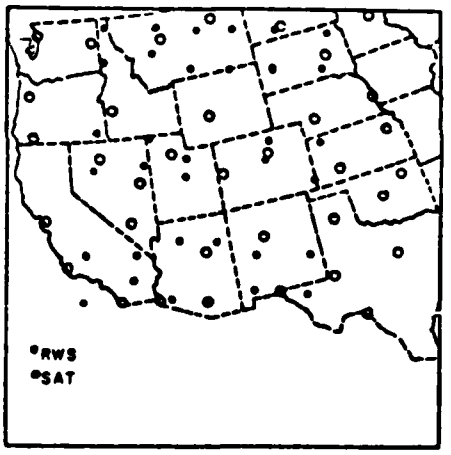

d. Area IV

Fig. 1. Distribution of rawinsonde (RWS) and Nimbus-6 soundings for Areas I-IV.

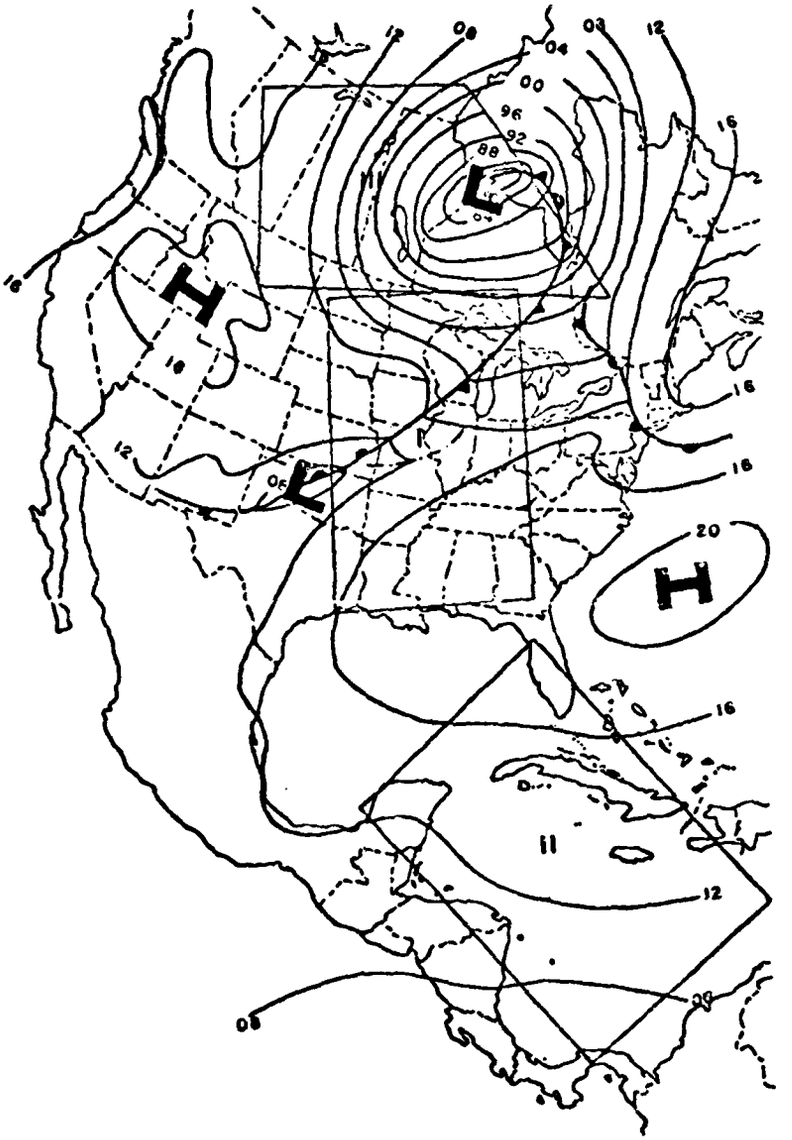

Fig. 2. Surface map covering Areas I, II, and III at 1800 GMT on 25 August 1975 (contours in millibars with first one or two digits omitted).

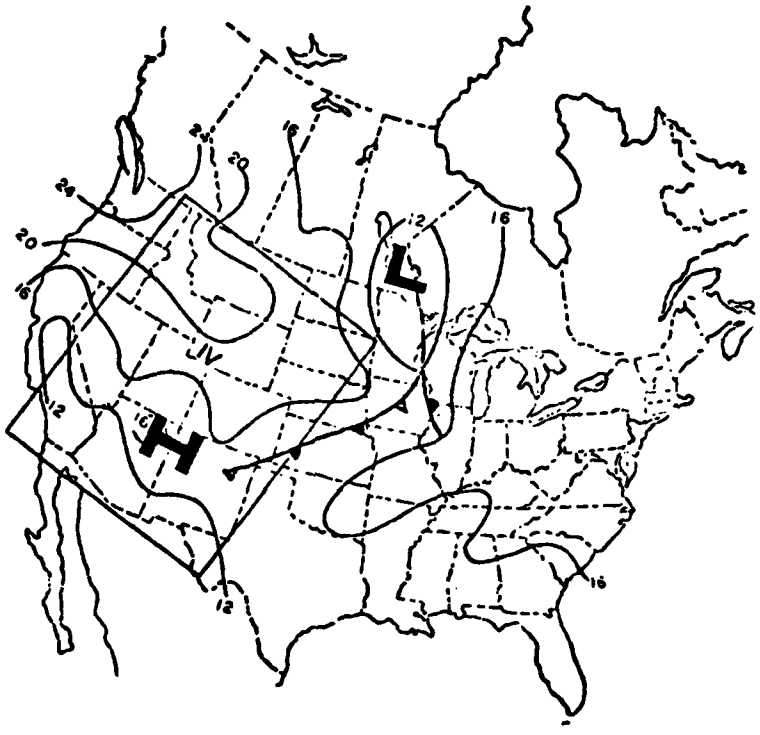

Fig. 3. Surface map covering Area IV at 0600 GMT on 3 September 1975 (contours in millibars with first two digits omitted).

Synoptic conditions at 1700 GMT on 5 February 1976 (not shown) include a high-pressure cell centered over the Atlantic Ocean to the east of South Carolina and a stationary front extending from West Virginia in a southwestward direction to central Texas. There were strong gradients of temperature and dew-point temperature across the front in Area V (central United States). Flow in Area VI (Caribbean) was dominated by the high-pressure cell and this area had relatively weak gradients of temperature and pressure. At this time, there was no low-pressure center in Canada as was present on 25 August 1975, so that the flow was generally from the northwest in Area VII. Temperature gradients in Area VII were intermediate between those of Areas V and VI.

The surface map for Area VIII at 2100 GMT on 10 April 1979 is shown in Fig. 4. At this time, a low-pressure system was centered in Colorado. A surface cold front extended from the low across Colorado, New Mexico, and Texas into Mexico. A warm front extended through eastern Texas across Louisiana and Florida. Temperature gradients were moderate in most of the

area of interest. Thunderstorms were reported along and in front of the cold front and much of the area was experiencing showers.

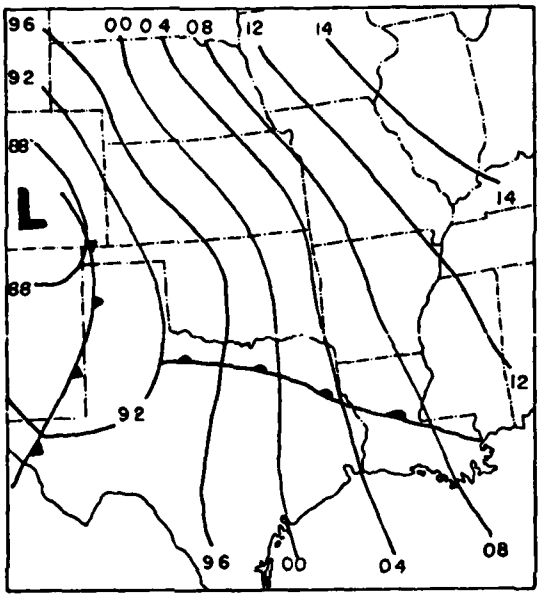

Fig. 4. Surface map covering Area VIII at 2100 GMT on 10 April 1979 (contours in millibars with first one or two digits omitted).

4. INTER-AREA ANALYSIS OF THE DISCREPANCIES BETWEEN RAWINSONDE AND NIMBUS-6 DATA

4.1 Approach

The general approach to the analysis of both the rawinsonde and satellite data and the comparisons between the two data sets is as follows. Satellite soundings were compared with the closest sounding location by determining the best estimate of the rawinsonde sounding at the time and location of the satellite sounding. This was done by a linear interpolation (in time) of the rawinsonde sounding using the two observations on either side of the satellite sounding. The plotted soundings and the results obtained by comparing satellite soundings with rawinsonde soundings made at standard release times indicated that this was the best approach. Data from the satellite and average rawinsonde soundings for selected constant-pressure surfaces then were placed onto a grid objectively by computer and selected parameters computed from the gridded data. The gridded fields were treated statistically or analyzed and compared. In addition, comparisons were made between selected vertical cross sections of rawinsonde and satellite data.

4.2 Analysis of Discrepancies Between Rawinsonde and Nimbus-6 Profile Parameters

For the purpose of comparison, rawinsonde soundings were paired with the closest satellite soundings. Not all satellite data were used since there were more satellite than rawinsonde soundings. Seven parameters were considered in this study: temperature, dew-point temperature, mixing ratio, thickness, lapse rate of temperature, precipitable water, and stability. Discrepancies between satellite and rawinsonde data for all seven parameters were computed by subtracting rawinsonde from satellite values. Computations were made for each level (e.g., temperature), or each layer (e.g., thickness), for each sounding. Additionally, discrepancies were stratified into three layers: 1000 to 500 mb, 500 to 300 mb, and 300 to 100 mb.

Cumulative probability frequency distributions of the discrepancies were computed for each layer for temperature, dew-point temperature, thickness, lapse rate of temperature, and mixing ratio for the ensemble of all paired points within each layer.

4.2.1 Temperature

Table 2 shows the mean and standard deviation of the mean discrepancy, the absolute mean discrepancy, and the root-mean-square discrepancy (RMSD) between Nimbus-6 and rawinsonde temperatures for Areas I-VII. The statistics were obtained from the lumped discrepancies for all levels reported for each station and for all stations in each area to provide a single set of criteria by which to judge the results of the comparisons.

The mean discrepancy in temperature has an average which ranges from 0.2 to 1.5°C and a standard deviation which ranges from 0.4 to 1.0°C. This indicates that Nimbus-6 temperatures may be either higher or lower than rawinsonde-observed temperatures, but each algebraic mean is a small positive number when averaged through the vertical column from the surface to 100 mb and over the whole area. The mean RMSD ranges from 1.1 to 3.2°C with largest magnitude in Area V. This may be due to the degradation of the HIRS data or changes in the meteorological conditions.

The means and standard deviations of temperature discrepancies for the 1000 to 500-, 500 to 300-, and 300 to 100-mb layers are shown in Table 3 for Areas I-VII. Mean discrepancies may be either positive or negative in the lowest layer, but are generally positive in the middle layer and are positive in the upper layer in all seven areas. This indicates that satellite-derived temperatures become increasingly higher, in general, than rawinsonde observed temperatures as higher layers are considered. Magnitudes of the standard deviation range from 0.8 to 3.7°C and are generally smallest over the water (Areas II and VI). Smallest standard deviations for each area generally are found in the middle layer, with the largest value in the upper troposphere, i.e., tropopause region. Staelin et al. (1973) have shown similar results, and Smith et al. (1975) have shown that in the troposphere the discrepancies between satellite and rawinsonde soundings were generally small except in the tropopause region between 300 and 100 mb. Their results are in agreement with those presented in this study.

The cumulative frequency distributions of the discrepancies in temperature are presented in Fig. 5 for Area I. The distributions are approximately normal (straight lines) except near the extremes. The small sample size is inadequate for defining extremes of the distributions.

Table 2. Mean ($\bar{x}$) and standard deviation (σ), lumped for all levels reported for each station and for all stations in each area, of the mean discrepancy ($\bar{\delta}$), the absolute mean discrepancy ($|\bar{\delta}|$), and the root-mean-square discrepancy (RMSD), in degrees Celsius, between Nimbus-6- and rawinsonde-derived temperatures and dew points [$\delta \equiv (T_{sat} - \bar{T}_{rws})$].

		Temperature			Dew-Point Temperature			Station Pairs
		$\bar{\delta}$	$\lvert\bar{\delta}\rvert$	RMSD	$\bar{\delta}$	$\lvert\bar{\delta}\rvert$	RMSD	
I[1] Central U. S. 8/25/75	$\bar{x}$	0.3	1.6	2.0	2.9	6.0	7.3	21
	σ	0.7	0.5	0.6	3.8	2.2	2.5	
V[3] Central U. S. 2/5/76	$\bar{x}$	1.5	2.4	3.2	2.3	7.2	8.3	18
	σ	1.0	0.9	1.3	6.1	3.6	4.2	
II[1] Caribbean 8/25/75	$\bar{x}$	0.2	0.9	1.1	2.8	5.4	6.6	9
	σ	0.4	0.2	0.2	3.2	2.0	2.6	
VI[3] Caribbean 2/5/76	$\bar{x}$	0.6	2.0	2.3	6.7	8.3	10.5	9
	σ	0.6	0.7	0.7	5.8	4.0	5.1	
III[1] Canada 8/25/75	$\bar{x}$	0.2	1.9	2.3	-2.0	5.5	6.8	7
	σ	1.0	1.0	1.0	4.6	2.2	2.2	
VII[3] Canada 2/5/76	$\bar{x}$	0.2	2.6	3.0	-12.9	14.7	16.5	7
	σ	0.7	1.1	1.2	9.6	7.6	8.5	
IV[2] Western U. S. 9/3/75	$\bar{x}$	0.4	1.8	2.2	6.7	8.8	9.9	23
	σ	0.8	0.6	0.7	7.0	5.4	5.3	

[1]Twenty-one levels from 1000 to 100 mb for temperature, 15 levels from 1000 to 300 mb for dew point.

[2]Sixteen levels from 700 to 100 mb for temperature, 10 levels from 700 to 300 mb for dew point.

[3]Ten levels from 1000 to 100 mb for temperature,5 levels from 1000 to 300 mb for dew point.

Table 3. Means and standard deviations of discrepancies (SAT-$\overline{\text{RWS}}$) between satellite and weighted rawinsonde data for selected parameters, by layer, synoptic situation, and geographical area.

		Central United States						Caribbean						Canada						Western U. S.		
		17Z 25 Aug 1975			17Z 05 Feb 1976			17Z 25 Aug 1975			17Z 05 Feb 1976			17Z 25 Aug 1975			17Z 05 Feb 1976			07Z 03 Sep 1975		
		A[1]	B[2]	C[3]	A	B	C	A	B	C	A	B	C	A	B	C	A	B	C	A	B	C
Temperature (°C)	Mean	-0.5	0.5	1.3	2.3	0.7	1.2	-0.1	0.5	0.3	0.9	2.8	0.0	0.1	-0.4	0.8	-0.4	-0.0	0.6	-1.6	0.0	1.8
	Standard deviation	1.8	1.3	2.3	3.7	2.0	2.7	1.1	0.8	1.3	1.4	1.6	2.9	2.5	2.0	2.6	3.6	3.4	2.6	2.6	1.5	2.0
	No. of data points	189	124	140	63	54	87	90	54	55	36	26	42	61	42	49	23	21	35	160	138	157
Dew point[4] (°C)	Mean	1.6	4.7		2.9	3.0		1.7	5.8		4.7	13.6		-2.0	-2.2		-11.9	-3.7		4.9	7.7	
	Standard deviation	5.8	8.7		9.3	9.6		6.2	7.0		7.3	9.7		5.2	9.0		13.4	8.4		6.9	9.8	
	No. of data points	189	120		61	36		90	52		33	19		60	32		20	6		157	127	
Lapse rate (°C/km)	Mean	-0.1	0.0	-0.3	0.7	-0.4	0.2	-0.1	-0.1	-0.0	-0.3	-0.0	0.8	0.1	-0.1	-0.1	0.0	-0.3	0.2	-0.7	-0.3	-0.3
	Standard deviation	1.3	0.7	1.4	1.7	1.0	1.3	0.9	0.4	0.8	0.5	0.8	1.2	1.4	0.8	1.4	0.8	1.6	1.4	1.9	0.7	1.1
	No. of data points	168	123	119	43	54	69	81	53	44	26	25	31	54	42	42	14	21	28	137	138	134
Mixing ratio[5] (gm/kgm)	Mean	0.2	0.1		-0.0			-0.5	0.2		0.6			-0.3	-0.0		-0.3			0.8	0.2	
	Standard deviation	1.8	0.6		1.8			2.1	0.6		1.3			1.5	0.2		0.3			1.5	0.5	
	No. of data points	189	120		61			90	52		33			60	32		20			157	127	
Precipitable water (mm)	Mean		0.7			0.5			-0.3			2.0			-0.6			0.2			1.1	
	Standard deviation		2.4			2.6			2.4			2.0			2.2			0.3			1.7	
	No. paired profiles		21			18			9			9			7			7			23	

[1]A = 1000-500 mb
[2]B = 500-300 mb
[3]C = 300-100 mb
[4]Dew-point data missing above 300 mb.
[5]Mixing ratio data missing above 300 mb.

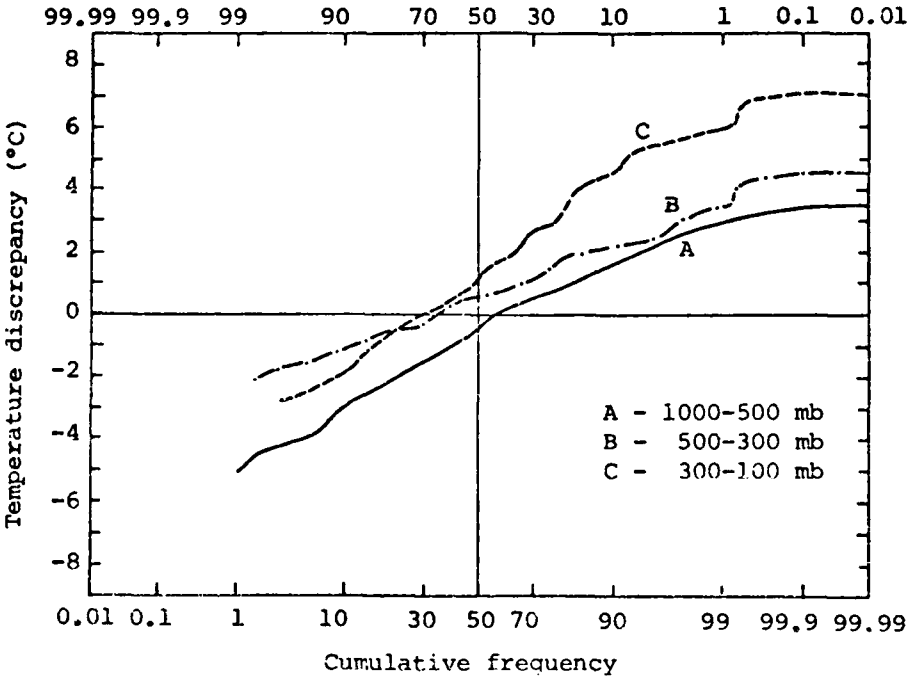

Fig. 5. Cumulative frequency distributions of discrepancies between satellite and rawinsonde temperatures by layer for Area I.

The tendency for the cumulative frequency distributions to be straight lines when plotted on probability paper suggests that the discrepancies between satellite and rawinsonde temperatures are due to random errors.

Cumulative frequency distributions for Areas II-VII (not shown) reveal that the discrepancies for temperature are nearly normal for all areas and all layers; that for dew-point temperature the lines are not as straight as for temperature but to a first approximation may be considered straight; that for mixing ratio the distributions tend to be normal in the two lower layers (data were not tabulated for the upper layer because of the absence of data) except on the tails of the distributions; and that the discrepancies for the lapse rate of temperature within the three layers may be considered normally distributed.

4.2.2 Dew-point Temperature

The Nimbus-6 soundings of dew-point temperature do not appear to be as reliable as those of temperature for any of the seven areas. Table 2 shows the mean discrepancies and mean RMS discrepancies for the vertical column 1000 to 300 mb for the seven areas. The mean RMS discrepancies range between 6.6°C (Area II) and 9.9°C (Area IV) in the first four

regions, and vary from 8.3 to 16.5°C in Areas V-VII. Considering only those areas with good quality HIRS data (Areas I-IV), the greatest disagreement is found for the western United States where the air had an extremely low water vapor content.

Discrepancies in dew-point temperature were examined for the 1000 to 500- and 500 to 300-mb layers. Means and standard deviations of the discrepancies within the two layers for all seven areas are shown in Table 3. Large biases (mean differences) exist in the satellite data relative to the rawinsonde data. With the exception of Area VII, the mean difference is smaller in the lower layer than in the upper layer. This may be attributable to the higher moisture content in the lower layer than in the upper layer where the data were considerably noisier than in the lower layer. Magnitudes of the standard deviation range from 5.2 to 13.4°C and indicate large dispersions of the discrepancies for each layer.

4.2.3 Thickness

Thickness was computed from the satellite and rawinsonde data according to

$$\Delta z = \frac{R\bar{T}^*}{g} \ln(p_1/p_2)$$

where R is the gas constant for dry air, $\bar{T}^*$ the mean virtual temperature in the layer between pressures p_1 and p_2, and g is the acceleration due to gravity. Here $\bar{T}^*$ is given by

$$\bar{T}^* = \bar{T} + \bar{w}/6$$

where $\bar{w}$ is the mean mixing ratio for the layer as determined from skew T-log p plots of rawinsonde and satellite profile data.

Layer thickness discrepancies were stratified into three layers, i.e., 1000 to 500 mb, 500 to 300 mb, and 300 to 100 mb. The thickness discrepancies were normalized to units of m km^{-1} because of the variable thickness of the layers. Means and standard deviations of normalized discrepancies in thickness are presented in Table 4 for Areas I-IV. Mean differences in normalized thickness are similar to those for temperature presented in Table 3. The best agreement between satellite and rawinsonde-derived thicknesses, indicated by the standard deviation of the differences, occurs in the middle layer, and the poorest in the upper layer (tropopause region). The smallest discrepancies occurred over water (Area II).

Table 4. Means and standard deviations of normalized discrepancies in thickness (m km^{-1}) for the layers surface to 500 mb, 500 to 300 mb, and 300 to 100 mb for Areas I-IV.

	Area I			Area II			Area III			Area IV		
	A	B	C	A	B	C	A	B	C	A	B	C
Mean	-1.8	1.9	6.0	-0.3	1.9	1.5	0.3	-1.5	3.6	-5.4	-0.4	8.1
St. Dev.	6.2	4.8	10.0	3.3	2.8	4.6	8.9	7.5	10.1	8.1	5.7	8.3
No. of data	169	124	140	81	54	54	54	42	49	138	138	157

4.2.4 Mixing Ratio

Mixing ratio values were obtained from dew-point temperature data plotted on skew T-log p diagrams for rawinsonde and satellite soundings. Mixing ratio data were stratified into two layers: 1000 to 500 mb and 500 to 300 mb. The results of comparisons between satellite and rawinsonde-derived mixing ratios are presented in Table 3. The means and standard deviations of the discrepancies in the lower layer are greater than those in the upper layer for all areas. These results were due to the lower moisture content in the upper layer where the data were considerably noisier than in the lower layer. Satellite-derived mixing ratios had a negative bias relative to rawinsonde-derived values in the lower layers of Areas II, III, and VII.

4.2.5 Precipitable Water

Precipitable water was computed by use of the equation

$$w = g^{-1} \int_{p_1}^{p_2} \bar{w}\, dp$$

where w is the precipitable water and the other symbols are as before. Precipitable water was computed by integrating the mixing ratio profile from 1000 to 300 mb. A mean RMS discrepancy between profile pairs for Areas I-IV of only 0.23 cm was found. This is somewhat better than the 0.5 cm RMS found by Hillger and Von der Haar (1977), presumably because of the microwave channels on Nimbus-6.

Means and standard deviations of discrepancies in precipitable water for Areas I-VII are shown in Table 3. The results for these areas show that average precipitable water may be obtained from satellite data with an accuracy of about 1 mm or less which is quite acceptable in most cases. The means were negative only in two areas. The standard deviations in Areas I-IV were quite consistent with a value around 2.3 mm except for Area IV (western United States) where the moisture content was low. Results obtained for Areas V and VI are similar to those found in Areas I-IV while those obtained for Area VII are much smaller.

4.2.6 Lapse Rate of Temperature

Lapse rates computed from Nimbus-6 and rawinsonde data were normalized to units of °C km^{-1}. Discrepancies in lapse rate were stratified into three layers.

Statistics for the differences between satellite and rawinsonde lapse rate data are shown in Table 3 for all seven areas. In Areas I-IV, biases in the differences are within 0.3°C km^{-1} except for Area IV where the bias is -0.7°C km^{-1} in the lowest layer. This large discrepancy is caused by errors in the satellite data near the ground over the mountains. The smallest standard deviation occurred in the middle layer of each of the first four areas with the lowest value over water (Area II). Normalized results obtained for Areas V-VII are similar to those for Areas I-IV except the smallest magnitude of the standard deviation did not consistently occur in the middle layer. This is probably due to the use of only ten levels of data in Areas V-VII.

4.2.7 Stability

Showalter and vertical totals indexes were computed for each satellite and rawinsonde sounding. Discrepancies between satellite and rawinsonde-derived indexes were computed by subtracting rawinsonde from satellite values. The average and standard deviation of the differences in each stability index were then computed for Areas I-IV.

It was found that all Showalter indexes computed from satellite data were positive. This is not fully understood but may be related to the temperature and moisture structure of the areas studied, or to the inaccuracies in satellite dew-point and ambient temperatures in the lower

troposphere. The average and standard deviation of the differences in Showalter indexes are 0.3 and 3.6, 1.4 and 2.8, 0.7 and 2.9, and -1.1 and 3.8 for Areas I, II, III, and IV, respectively.

Smaller percentage errors in the mean discrepancies were found for the vertical totals index than for the Showalter index. The average and standard deviation of the differences in the vertical totals index are -2.1 and 2.0, -1.1 and 0.5, 0.4 and 3.1, and -1.6 and 4.1 for Areas I, II, III, and IV, respectively. The vertical totals indexes obtained from satellite data differ from those obtained from rawinsonde data by less than 5%. This good agreement between satellite and rawinsonde data again reflects the high quality of the satellite temperature data.

4.3 Analysis of Discrepancies Between Rawinsonde and Nimbus-6 Data on Constant-Pressure Surfaces

4.3.1 Analysis Procedure

An objective analysis scheme developed by Barnes (1964) was used to interpolate rawinsonde and satellite data to a square grid of 324 points with a grid-point spacing of 158 km. The gridding procedure is iterated four times and a scanning radius determines the maximum distance that a data point may influence the grid-point values. A nine-point smoothing routine (Shuman, 1957) was applied to each gridded field to reduce effects of spurious variations. The gridding procedure, when used with the proper scanning radius and the smoothing routine, produces fields of data which are similar to hand-analyzed charts. Locations of the grid points are shown in Fig. 6 for the central and western United States, Canada, and Caribbean areas.

After the grid was established, sounding data from the surface to 100 mb were placed on the grid for the particular area involved. Data sets were created with gridded surface fields of elevation, pressure, temperature, and dew-point temperature, and fields of temperature and dew-point temperature at each of the 21 pressure levels (10 in Areas V-VII) above the surface. This was done for both rawinsonde and satellite data. An auxiliary data set was created for rawinsonde-observed geopotential height, and observed u- and v-component wind data at the ten mandatory levels. The 1200 and 0000 GMT rawinsonde gridded values were interpolated to determine values corresponding to the time of the satellite data, at the

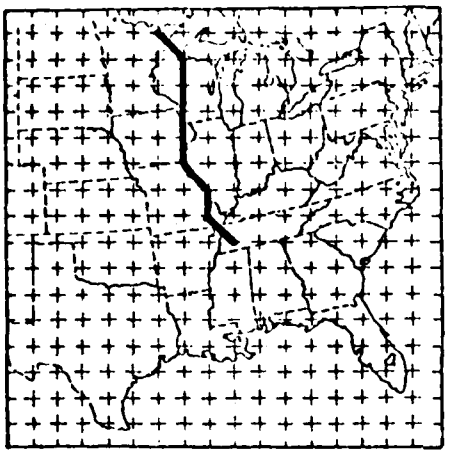

a. Central United States

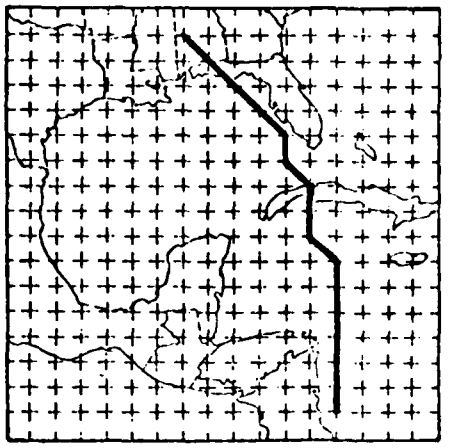

b. Caribbean

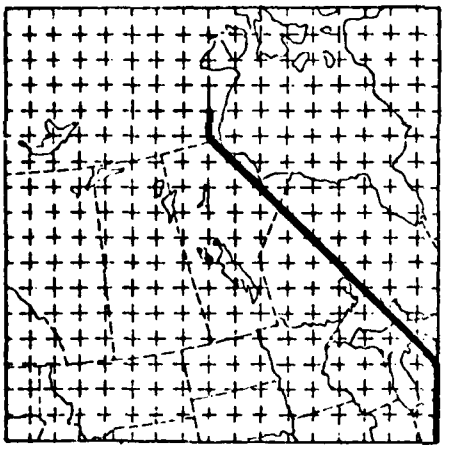

c. Canada

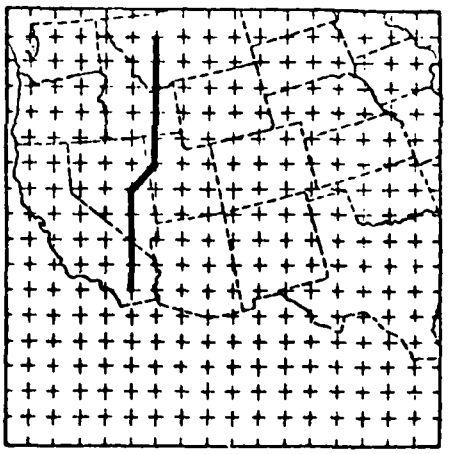

d. Western United States

Fig. 6. Locations of grid points and cross-sections for four geographic regions.

risk of incurring errors because of fast-moving map features.

Differences between satellite and rawinsonde values were computed by subtracting rawinsonde from satellite values at the grid points. The mean and standard deviation of the differences were prepared for nine constant-pressure surfaces (850, 700, 500, 400, 300, 250, 200, 150, and 100 mb). Vertical profiles of these statistics are presented for each parameter. Table 5 contains the means and standard deviations of differences for each parameter on the 700-, 500-, and 300-mb surfaces for Areas I-VII. An estimated average magnitude of each parameter is given in the table for the respective constant-pressure surface over the area. In cases where large gradients in the parameter were evident, two values appear that represent average values over portions of the area. The magnitudes of the parameters are included in order to provide some idea of the magnitudes of the differences compared to the parameter under consideration.

4.3.2 Temperature-related Variables

Profiles of the average and standard deviation of the differences between rawinsonde and Nimbus-6 temperatures are shown in Fig. 7 for Areas I-IV. The magnitudes of the average and standard deviation of the differences are relatively small in Area II, but are large with more vertical variation in Areas I and IV. Average values in Area III are less than 0.75°C except near the tropopause (250 mb), and magnitudes of the standard deviation are intermediate between those of Area II and those of Areas I and IV. The flat thermal field in the Caribbean, associated with the weak anticyclonic circulation and high tropopause, creates optimum conditions for accuracy in the satellite sounding data. Average differences tend to be largest near the tropopause in each of the first four areas. These results are similar to the 2°C RMS discrepancy for the lower troposphere found by Waters et al. (1975) for the NEMS instrument carried by the Nimbus-5 satellite, and are in close agreement with the 1.6°C RMS for the 1000-500 mb layer found by Wilcox and Sanders (1976).

Profiles of the average and standard deviation of the differences for lapse rate of temperature for Areas I-IV are shown in Fig. 8. These show that up to near 400 mb, the average and standard deviation of the differences are less than or equal to approximately 0.5°C km^{-1}. Due to the vertical smoothing in the satellite soundings, the change of vertical

Table 5. Means and standard deviations of differences between gridded satellite and weighted rawinsonde parameters on selected constant pressure surfaces for four geographical areas.

		Central United States						Caribbean					
		Area I			Area V			Area II			Area VI		
		700	500	300	700	500	300	700	500	300	700	500	300
Temperature (°C)	Mean	-0.7	0.4	0.3	1.4	-0.2	2.0	0.3	0.5	1.1	0.4	2.4	4.2
	Standard Deviation	1.5	1.3	1.8	2.3	2.9	5.0	0.5	0.7	0.4	0.7	0.7	0.8
	Approx. Magnitude	-1/9	-17/-35	-42/-38	-21/-10	-20/-15	-50/-44	8.5	-7	-33	6.5	-13	-40
Dew-point Temperature (°C)	Mean	1.6	1.7	-1.0	3.3	4.0	-	-2.5	14.0	6.3	3.7	9.5	-
	Standard Deviation	4.8	6.8	6.2	7.6	7.5	-	4.4	4.9	5.4	7.4	6.7	-
	Approx. Magnitude				-25/-11	-30/-40	-				-20	-35	-
Lapse Rate of Temperature ($°C\ km^{-1}$)	Mean	-0.5	-0.3	0.2	1.1	0.3	1.5	-0.3	-0.2	-0.0	-0.6	-0.6	0.2
	Standard Deviation	0.4	0.5	0.5	1.7	1.1	0.8	0.1	0.1	0.1	0.2	0.2	0.6
	Approx. Magnitude	6.2	6.5	7.4	5.8	6.8	8.0	6.0	6.2	7.6	6.0	6.7	6.7
Magnitude of Horizontal Gradient of Temperature (°C/1000 km)	Mean	-3.7	-0.3	0.4	-2.1	7.1	14.1	-1.4	-1.3	-0.6	-0.3	-0.6	-0.1
	Standard Deviation	4.5	3.6	5.1	8.1	19.5	36.5	1.1	1.5	1.1	2.2	2.6	3.5
	Approx. Magnitude	15/3	15/4	17/3	5/30	6/13	8	1	1	1	2	4	4
Geopotential Height (m)	Mean	7.4	4.8	5.1	23.4	21.7	30.4	-4.6	-1.0	11.7	10.1	33.4	80.6
	Standard Deviation	14.0	17.8	31.9	45.1	44.9	79.7	8.3	10.2	15.0	10.3	11.7	19.2
	Approx. Magnitude	3150	5820	9570	3100	5800	9400				3180	5880	9650
Zonal Wind Speed ($m\ s^{-1}$)	Mean	-0.6	-0.2	1.2	-3.1	-0.7	10.7	-0.4	1.1	-0.6	2.0	2.0	2.3
	Standard Deviation	5.1	7.3	11.1	13.0	13.9	31.6	5.1	5.8	7.6	6.5	6.3	11.1
	Approx. Magnitude	10	25/1	45/-5	14	20	28				-5/12	-12/15	-21/26
Meridional Wind Speed ($m\ s^{-1}$)	Mean	-2.3	-2.1	-3.6	2.5	1.3	-13.8	-0.2	-1.4	-3.5	3.7	-0.7	-0.7
	Standard Deviation	4.0	5.2	10.2	13.3	16.1	54.2	6.3	8.3	11.0	5.3	5.8	10.8
	Approx. Magnitude	8	20/5	35/5	8	12	14				-14/13	-2/16	-10/26
Scalar Wind Speed ($m\ s^{-1}$)	Mean	-0.7	-0.4	0.9	4.6	4.2	21.7	2.5	1.3	2.7	-2.9	0.8	1.6
	Standard Deviation	4.8	6.6	10.9	12.6	15.0	51.5	4.7	5.4	5.6	4.6	5.3	10.9
	Approx. Magnitude	15	28/6	45/7	18	20	28				10	12	20
Wind Direction (Deg)	Mean	-14.4	-13.9	-24.2	10.0	1.3	-9.3	-2.6	4.3	-11.3	12.9	-22.1	-8.1
	Standard Deviation	35.9	32.0	46.3	62.5	48.3	40.5	64.6	79.4	116	89.4	73.7	52.2
	Approx. Magnitude	225	250	230	240	250	240	*	*	*	140	180	200
No. of data points		90			137			58			83		

*Direction highly variable

Table 5. Continued.

		Canada Area III			Canada Area VII			Western U.S. Area IV		
		700	500	300	700	500	300	700	500	300
Temperature (°C)	Mean	0.2	-0.4	-0.3	4.2	0.1	1.0	-2.0	-0.5	0.8
	Standard Deviation	1.1	1.1	1.6	1.8	2.3	0.9	2.4	1.5	1.1
	Approx. Magnitude	-2	-16	-45	-24	-38	-52	13	-9	-35
Dew-point Temperature (°C)	Mean	-4.3	-3.1	-	1.7	3.7	-	3.6	7.5	-9.4
	Standard Deviation	3.8	6.0	-	8.4	4.9	-	4.0	7.5	12.5
	Approx. Magnitude				-30	-44				
Lapse Rate of Temperature (°C km^{-1})	Mean	0.1	0.1	-0.6	0.7	0.7	0.4	-	-0.4	-0.6
	Standard Deviation	0.4	0.3	0.7	1.4	1.1	1.2	-	0.6	0.5
	Approx. Magnitude	5.5	6.2	6.5	5.8	6.0	4.0	-	6.7	7.3
Magnitude of Horizontal Gradient of Temperature (°C/1000 km)	Mean	-0.4	-0.8	-1.6	2.2	3.4	0.4	-	-3.2	1.7
	Standard Deviation	4.1	3.2	4.4	4.2	6.4	2.9	-	6.4	3.3
	Approx. Magnitude	3.5	8	8	10	10	5		5	7
Geopotential Height (m)	Mean	1.3	-3.4	-10.0	27.0	56.2	62.7	-14.9	-26.7	-27.0
	Standard Deviation	23.2	23.5	32.0	31.3	41.6	27.2	17.0	24.6	27.5
	Approx. Magnitude				2400	5280	8600	3100	5860	9600
Zonal Wind Speed (m s^{-1})	Mean	0.5	1.4	3.0	3.5	3.8	-0.7	-1.7	-1.4	1.0
	Standard Deviation	7.0	8.4	11.7	6.8	10.3	11.1	4.8	8.0	12.1
	Approx. Magnitude				15	20	20	2	8	18
Meridional Wind Speed (m s^{-1})	Mean	-1.4	-2.0	-3.3	2.4	1.5	1.1	0.4	1.2	1.6
	Standard Deviation	7.8	7.2	7.0	4.9	8.2	10.3	4.8	6.7	9.7
	Approx. Magnitude				-5	-15/15	-25/25	2	4	9
Scalar Wind Speed (m s^{-1})	Mean	0.3	1.0	1.6	4.1	2.0	-1.9	0.3	0.1	2.6
	Standard Deviation	7.8	8.6	9.7	6.8	10.2	12.7	5.1	8.7	12.0
	Approx. Magnitude				15	25	30	3	9	18
Wind Direction (deg)	Mean	-2.8	0.3	-1.5	4.0	5.4	-1.4	3.4	8.8	4.3
	Standard Deviation	33.3	36.8	54.0	15.9	24.5	14.0	63.0	41.0	31.1
	Approx. Magnitude	*	*	*	300	280	280	180	230	250
No. of data points			87						100	

* [illegible]

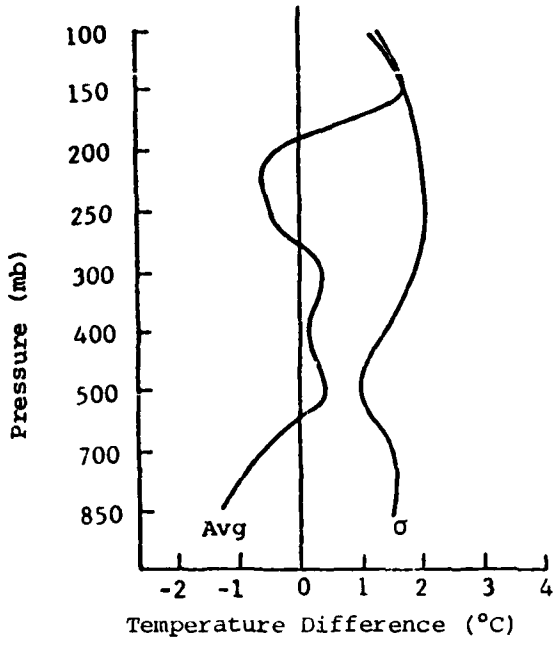

a. Area I

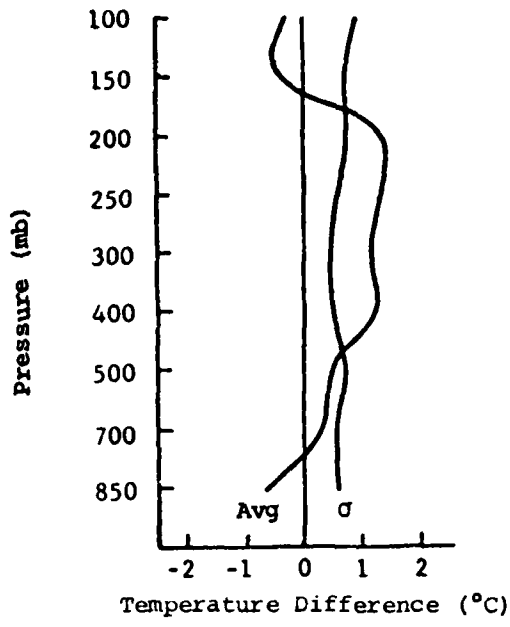

b. Area II

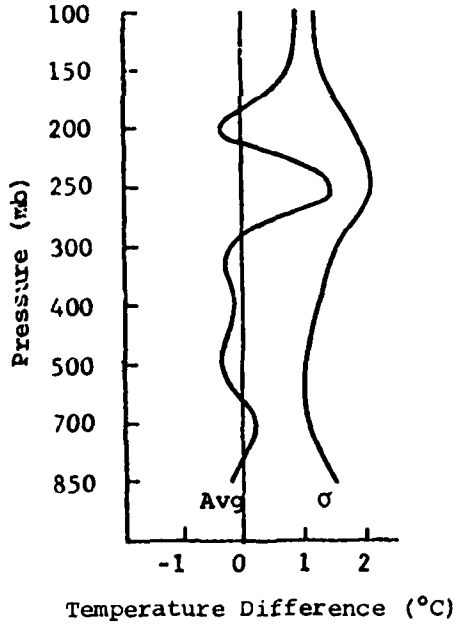

c. Area III

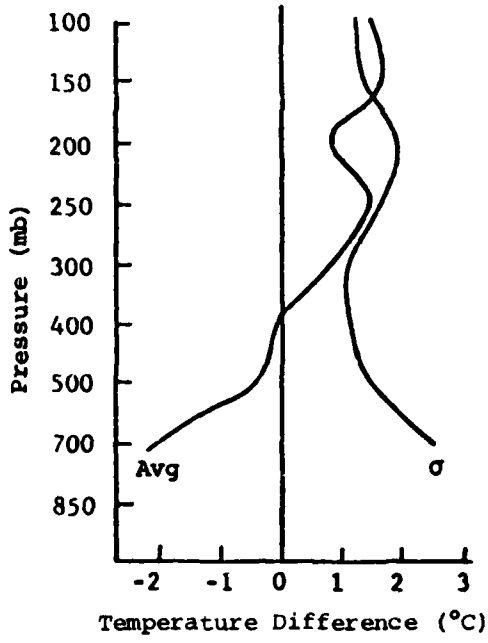

d. Area IV

Fig. 7. Profiles of the average difference and standard deviation of the differences between satellite and rawinsonde temperatures (satellite minus rawinsonde) for Areas I-IV.

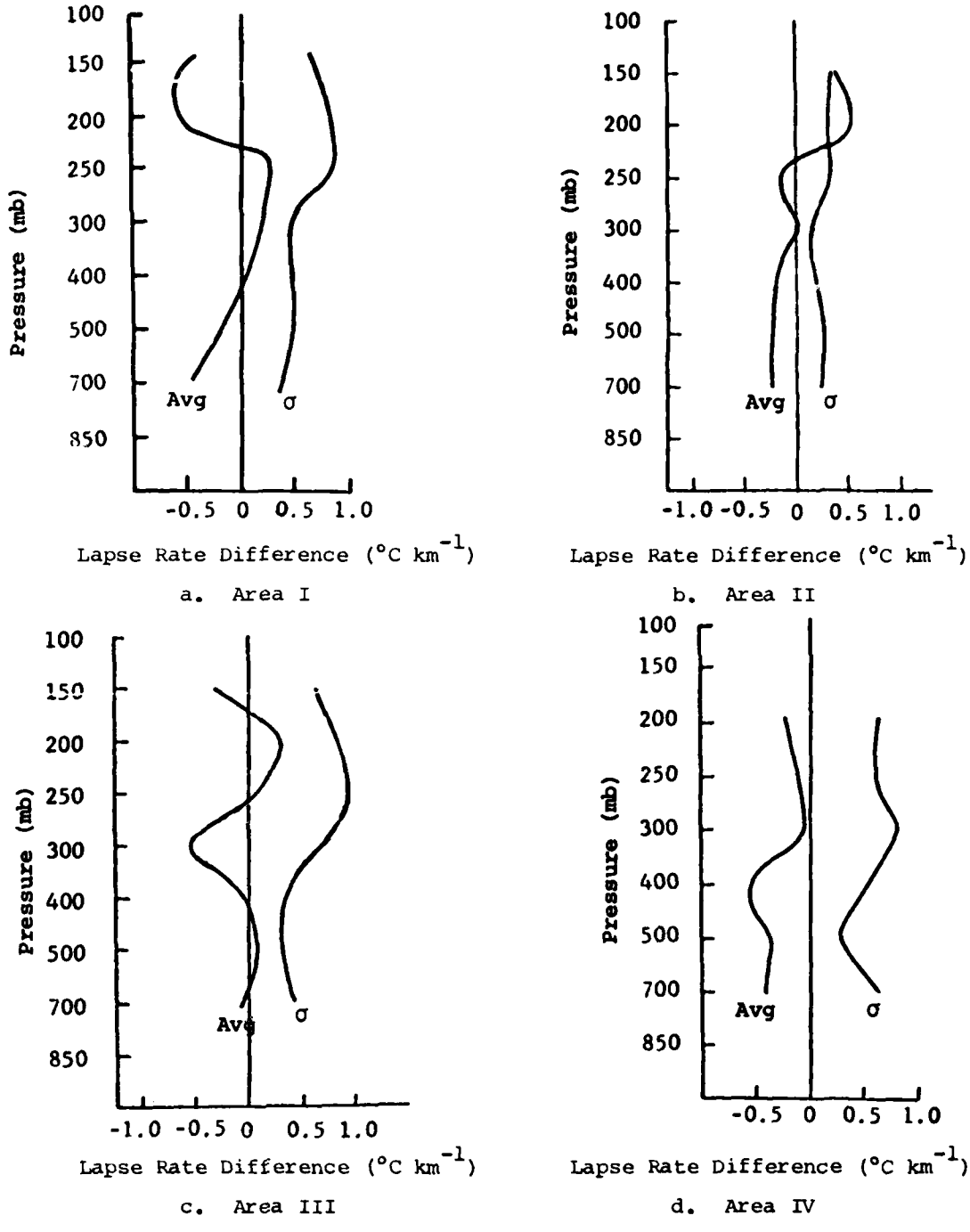

Fig. 8. Profiles of the average difference and standard deviation of the differences between satellite and rawinsonde vertical lapse rates of temperature (satellite minus rawinsonde) for Areas I-IV.

lapse rate of temperature in satellite data associated with the tropopause occurs over a deeper layer than the corresponding change in rawinsonde data, so that the satellite data indicate a decrease which begins at a lower level than that in rawinsonde data. Therefore, differences tend to be negative (satellite values too low) below the tropopause in each area, while approaching zero and perhaps changing sign above the cropopause. This trend is particularly evident in Area III where the sign of the average difference changes at 250 mb, the approximate level of the tropopause.

Vertical difference profiles for Areas I-IV for the horizontal gradient of temperature are shown in Fig. 9. Average differences are small, less than 2°C $(1000\ km)^{-1}$ in all four areas, while standard deviations are near 1.7°C $(1000\ km)^{-1}$ in Area II and are larger in Areas I, III, and IV where values reach 5°C $(1000\ km)^{-1}$. This is in direct association with the magnitudes of the horizontal temperature gradients in these areas. Area II (Caribbean) contains only small gradient values, thus allowing the differences there to be small; the polar front in Areas I and III causes gradients and differences to be somewhat larger. Average differences show that the satellite values are too small in Area III, too large in Area II, and vary in Areas I and IV from too small near the surface to too large through the middle and upper troposphere.

Results for Areas I-VII for temperature-related variables are presented in Table 5. The average and standard deviation of the differences in temperature, lapse rate of temperature, and horizontal gradient of temperature generally are larger in Areas V-VII than in the first four areas.

4.3.3 Dew-point temperature

Vertical difference profiles for dew-point temperature are shown in Fig. 10 for Areas I-IV. The standard deviation of the differences in Areas I and III averages approximately 5°C in the lower troposphere, while values of near 3.5°C and 7.5°C are typical for Areas II and IV, respectively. Differences in Area IV are somewhat larger than those in the other three areas with values increasing above 400 mb to near 10°C. In all areas except Area III, the satellite indicates too much moisture relative to the

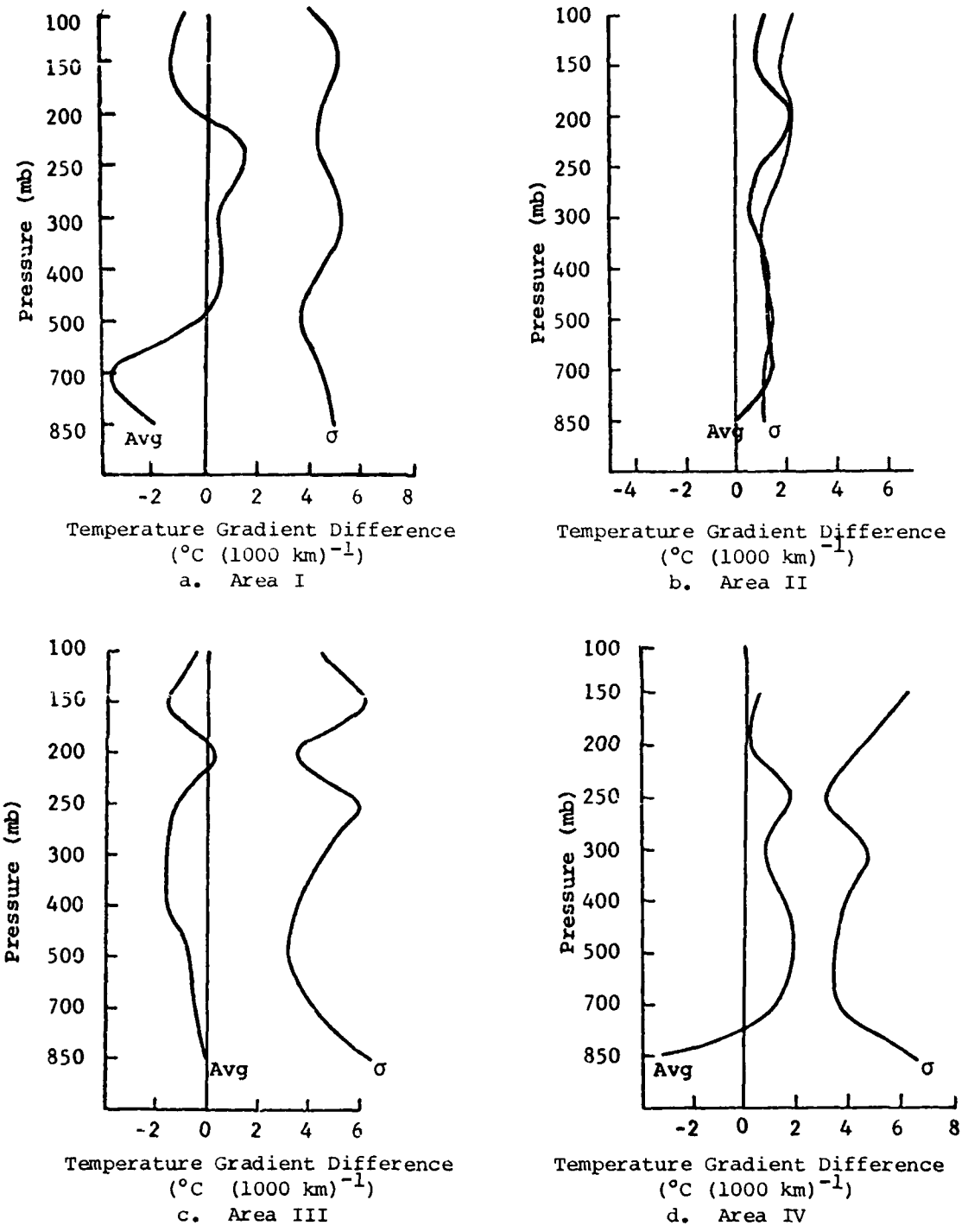

Fig. 9. Profiles of the average difference and standard deviation of the differences between satellite and rawinsonde horizontal temperature gradients (satellite minus rawinsonde) for Areas I-IV.

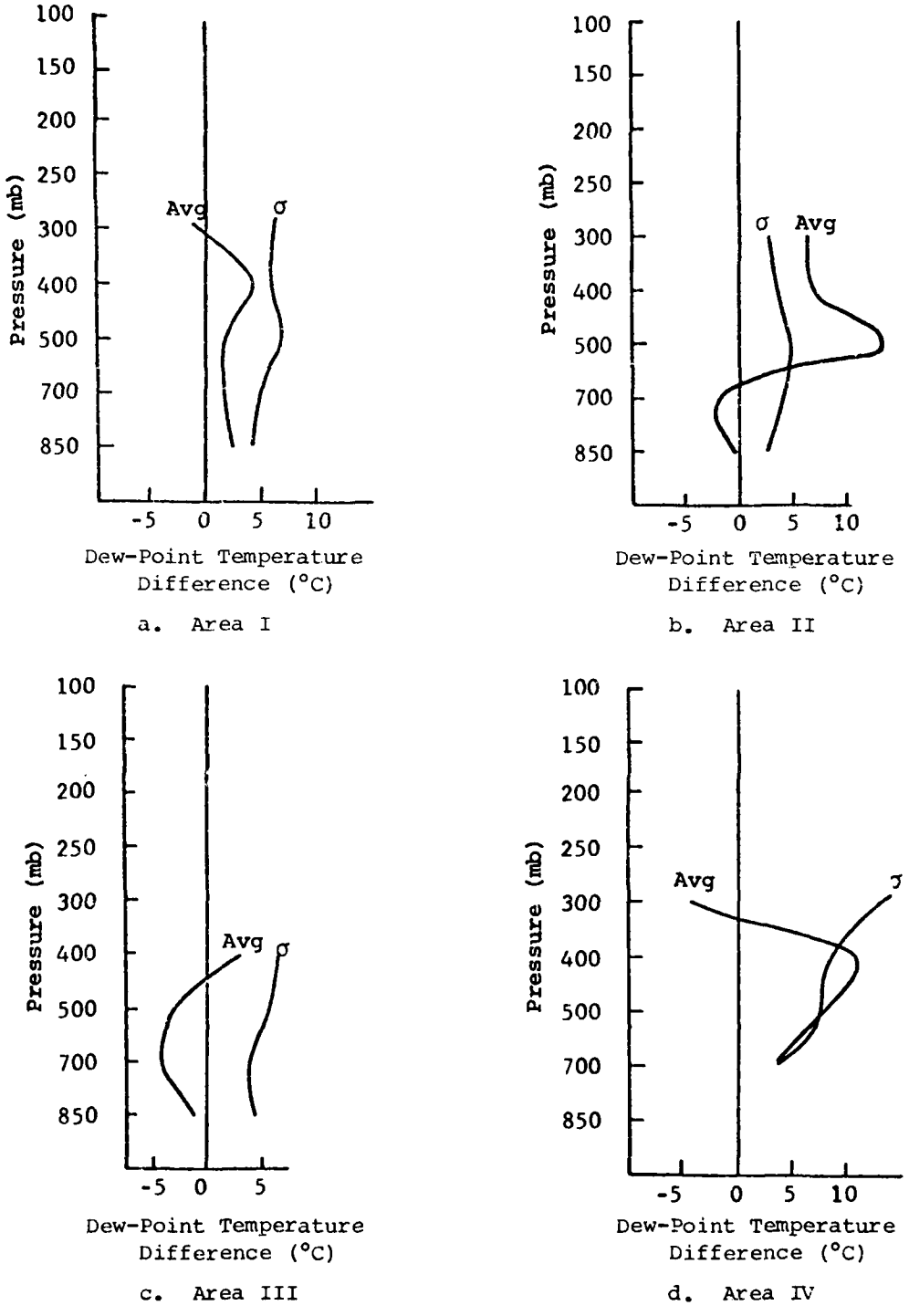

Fig. 10. Profiles of the average difference and standard deviation of the differences between satellite and rawinsonde dew-point temperatures (satellite minus rawinsonde) for Areas I-IV.

rawinsonde with positive average differences at most levels. Results obtained for Areas V-VII, shown in Table 5, indicate that Nimbus-6 dew-point temperatures on 5 February 1976 are of poorer quality than those obtained on 25 August 1975.

4.3.4 Geopotential Height and Geostrophic Wind

Geopotential height fields were computed from gridded satellite data by integrating the hydrostatic equation from the surface upward. In the integration process, mean virtual temperature for each layer was defined as the arithmetic average of the values at the top and bottom of the layer. Surface temperature and dew-point temperature were obtained from hourly synoptic data. Surface pressure was based on the altimeter setting reported in hourly teletype data and the height of the station as given in each satellite sounding.

Satellite-derived heights are compared to heights calculated by the National Weather Service and supplied at mandatory levels in teletype data. Vertical profiles of the differences in geopotential height are presented in Fig. 11 for Areas I-IV. Area II (Caribbean) exhibits the smallest differences between satellite and rawinsonde values, with standard deviations increasing from near 8 m at 850 mb to 16 m at 100 mb. Standard deviation values range from 12 to 56 m in Area I, from 18 to 50 m in Area IV, and from 28 to near 60 m in Area III with maximum values near 250 mb. Average differences are lower than standard deviations in all areas except Area II.

Profiles of the differences between geostrophic winds computed from rawinsonde and satellite geopotential heights are presented in Figs. 12 and 13 for the scalar wind speed and wind direction, respectively, for Areas I-IV. Average differences in wind speed are small in the lower layers, with values near 5 to 7 m s^{-1} near the tropopause. Standard deviations of differences in wind speed tend to increase with altitude, with values between 5 and 15 m s^{-1}. Differences near the tropopause tend to be larger than those elsewhere in all four areas. With the exception of Area II, the standard deviation of direction difference (Fig. 13) tends to average approximately 45°, and peaks near the tropopause. Area II (Caribbean) is quite different from the other cases due to the small wind speeds in that region.

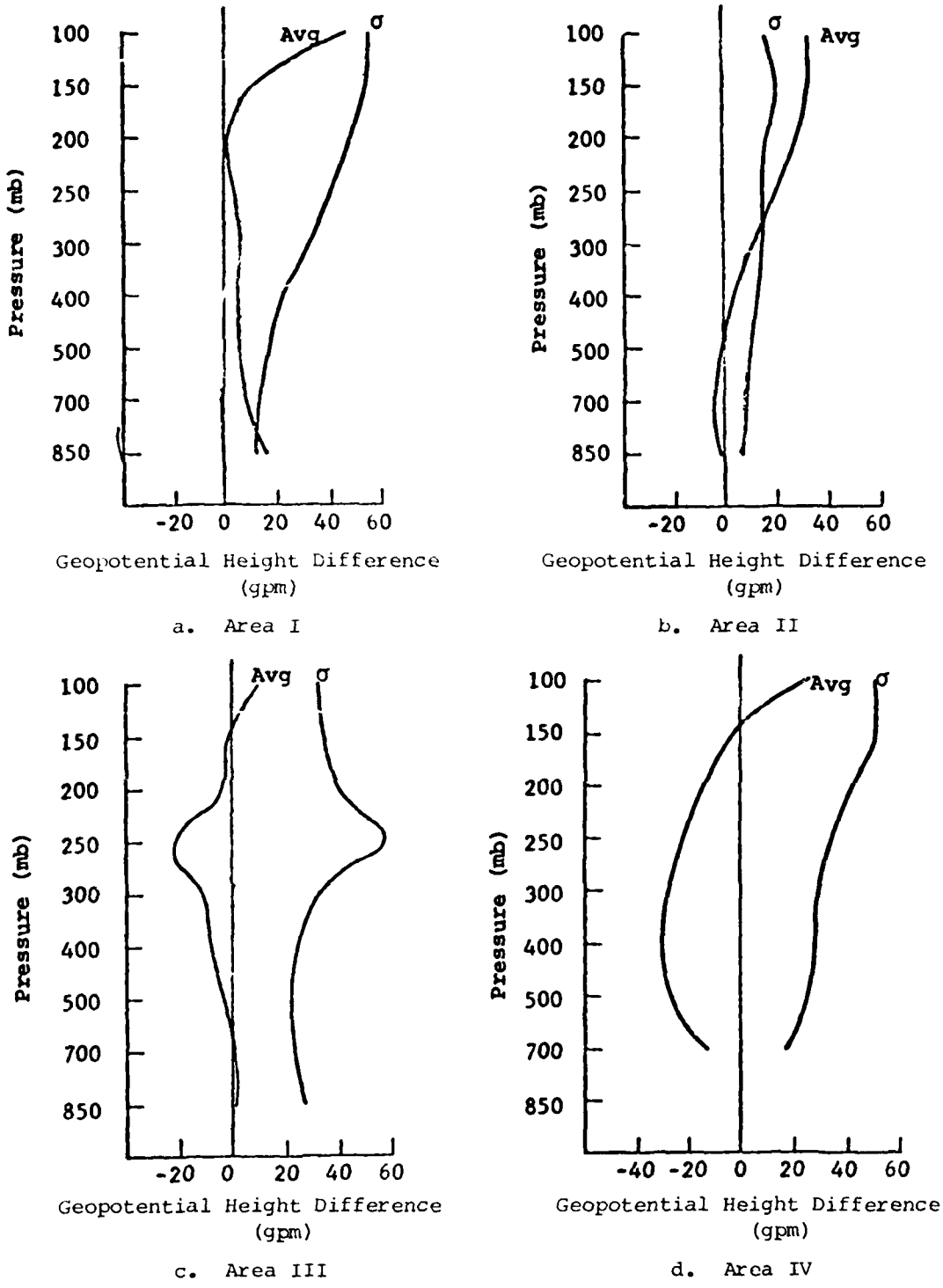

Fig. 11. Profiles of the average difference and standard deviation of the differences between satellite and rawinsonde geopotential heights (satellite minus rawinsonde) for Areas I-IV.

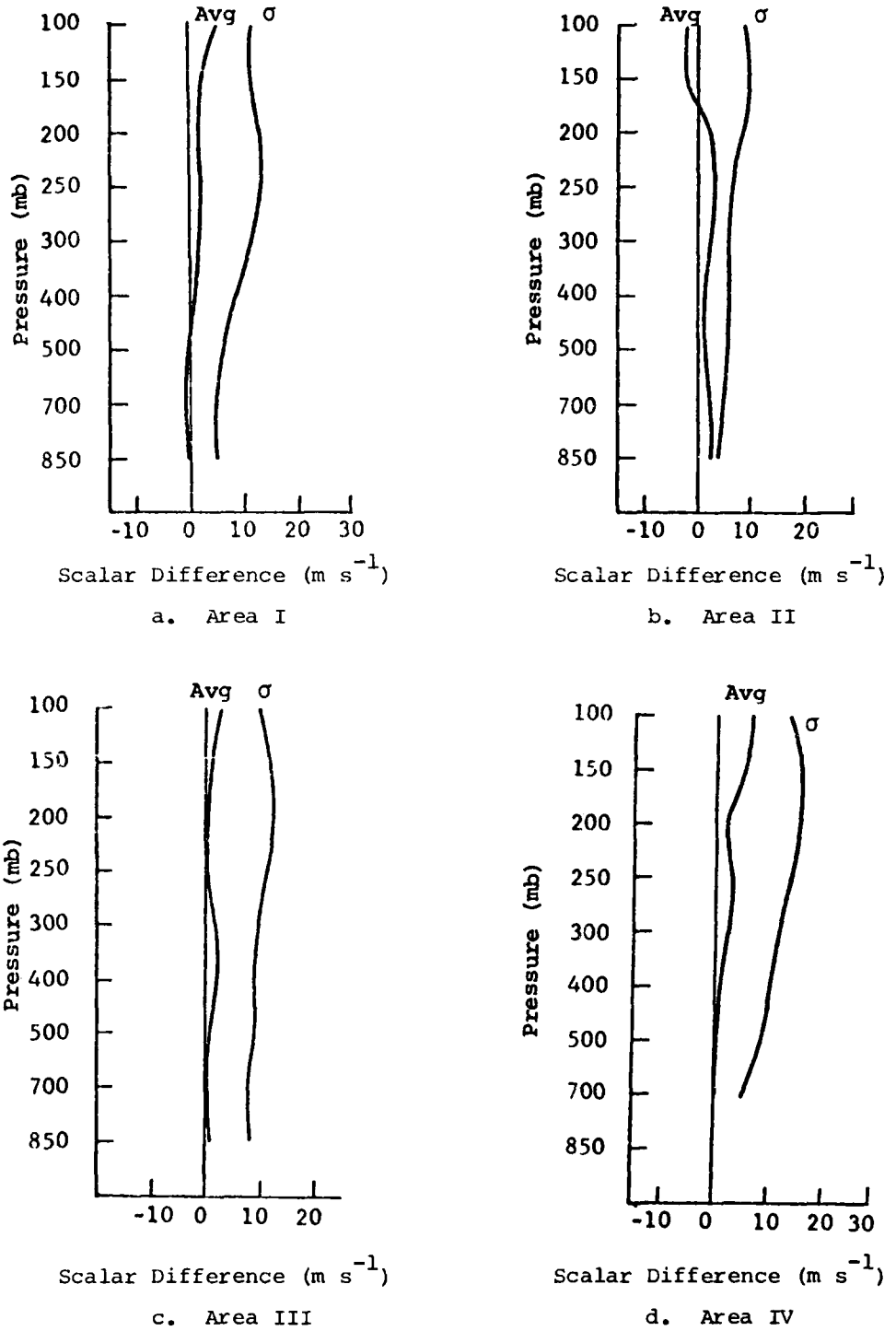

Fig. 12. Profiles of the average difference and standard deviation of the differences between satellite and rawinsonde geostrophic wind speeds (satellite minus rawinsonde) for Areas I-IV.

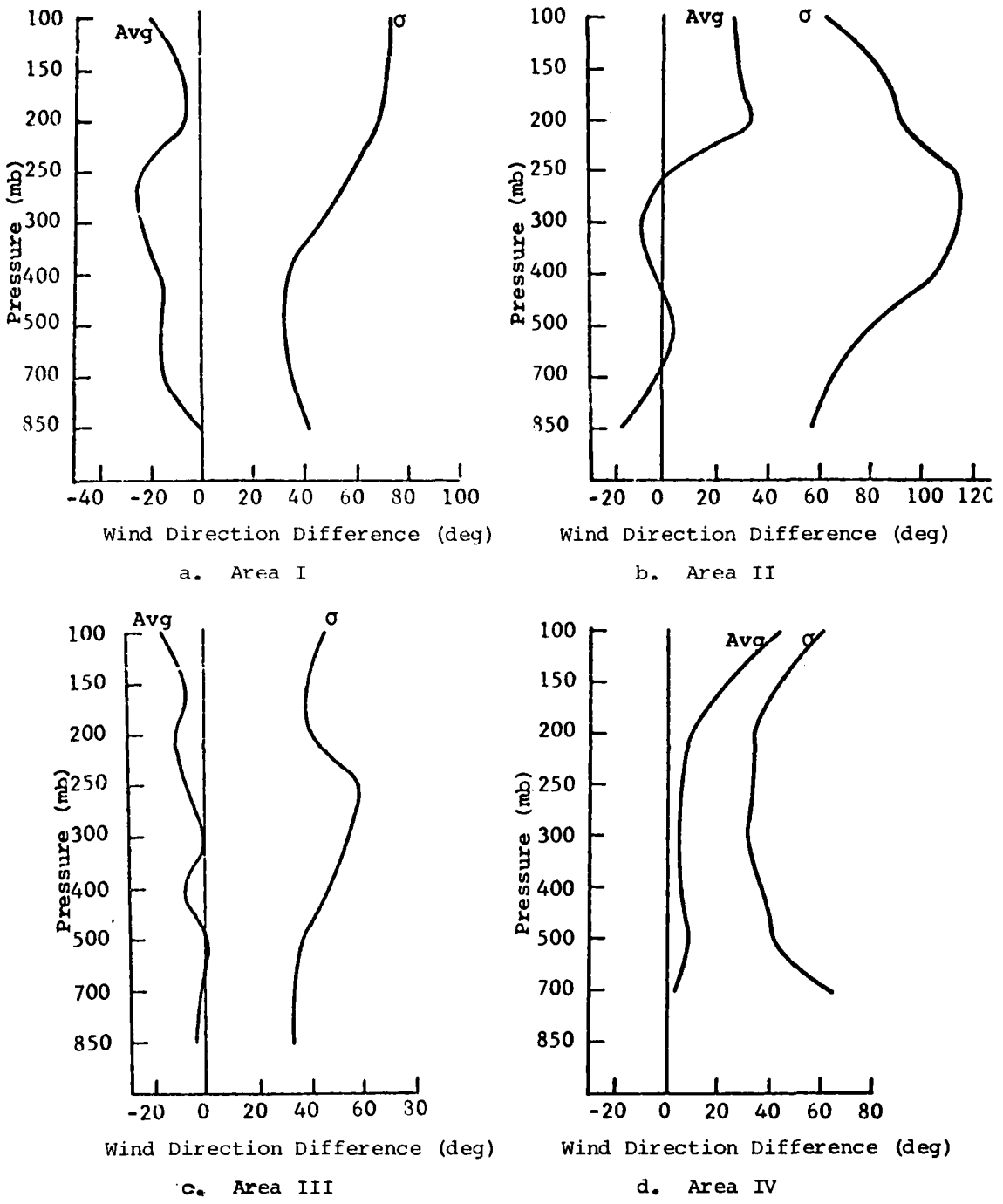

Fig. 13. Profiles of the average difference and standard deviation of the differences between satellite and rawinsonde geostrophic wind directions (satellite minus rawinsonde) for Areas I-IV.

Results obtained for geopotential height and geostrophic wind for Areas V-VII are presented in Table 5 along with those obtained for the first four areas. A comparison of the results from the two sets of areas indicate that the quality of satellite-derived geopotential height and geostrophic wind speed are poorer in Areas V-VII than in Areas I-IV. Large differences between satellite- and rawinsonde-derived fields may be due to the poor quality of the satellite sounding data and the use of ten-level satellite data in Areas V-VII.

5. SYNOPTIC STRUCTURE REVEALED BY RAWINSONDE AND NIMBUS-6 DATA

Analyzed constant-pressure charts and cross sections are presented for Area I (central United States on 25 August 1975). These were constructed from gridded data, and represent the horizontal and vertical variations of atmospheric parameters as depicted by satellite and rawinsonde data, as well as variations of quantitative differences between the two types of data.

5.1 Constant-pressure Charts

5.1.1 Temperature

Fields of temperature at 850 and 500 mb for Area I are presented in Fig. 14. There is a surface front across the northwest portion of the area (see Fig. 2) that corresponds to the higher-than-average temperature gradient which is apparent in both types of data in that part of the area. At 850 mb, rawinsonde temperatures range from near 16°C just south of the front to near 8°C north of the front, while satellite temperatures range from near 16°C south of the front to near 6°C north of the front. This set of charts shows that, while temperature differences are largest just south of the front over Missouri at 850 mb (near 4°C), a reasonable correspondence exists between satellite and rawinsonde temperature data. The sign of the differences seems to be related to the location of the front, since positive differences are to the north and negative differences to the south of the front.

It has been determined from analyzed charts for Areas I-IV that measurements of temperature obtained from satellite-observed radiancies are accurate enough to depict fronts on constant-pressure charts, although the contrast in satellite temperatures across the front is less than that in rawinsonde temperatures. Temperature patterns on constant-pressure charts from rawinsonde and Nimbus-6 data are similar.

5.1.2 Dew-point Temperature

Charts showing fields of satellite and rawinsonde dew-point temperatures for Area I at 850 mb are shown in Fig. 15. The satellite data are consistent with the rawinsonde data in terms of the general pattern, with indications of moist air south of the front and dry air north of the front. The gradients in dew-point in the satellite data at this level are not sufficient to provide precise indication of the frontal position. On the other hand, the front can be located fairly easily in the rawinsonde data

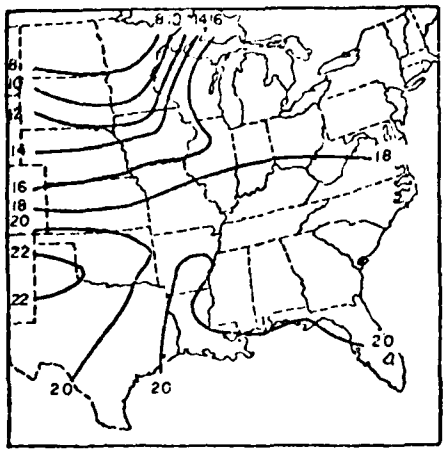

a. Rawinsonde (RW), 850 mb

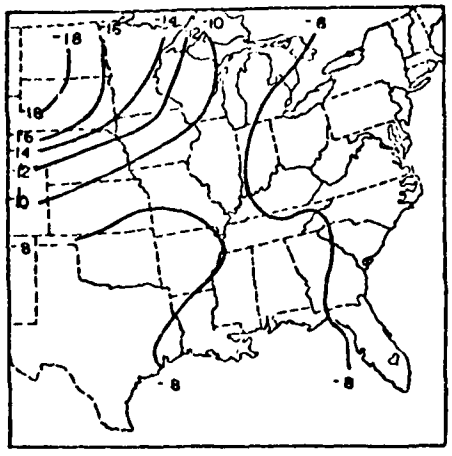

d. Rawinsonde (RW), 500 mb

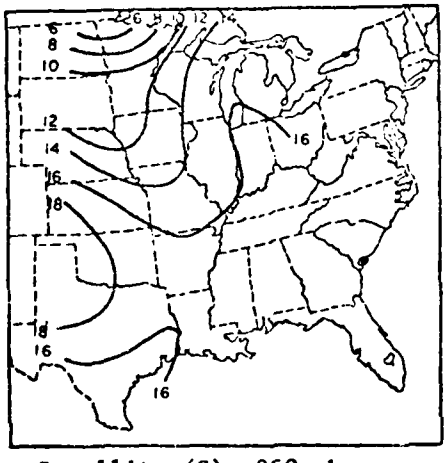

b. Satellite (S), 850 mb

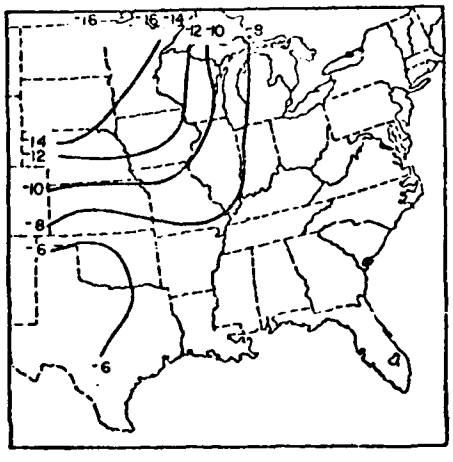

e. Satellite (S), 500 mb

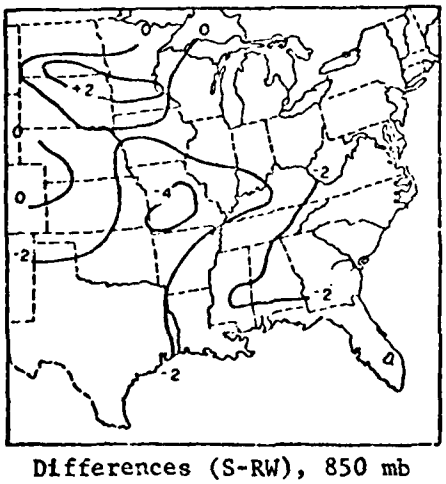

c. Differences (S-RW), 850 mb

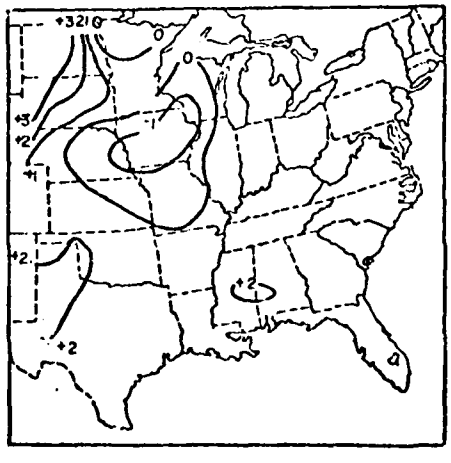

f. Differences (S-RW),500 mb

Fig. 14. Charts of temperature and temperature difference (°C) at 850 and 500 mb over the central United States region (Area I).

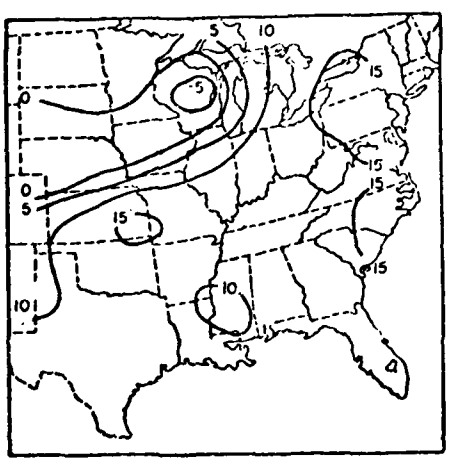

a. Rawinsonde (RW), 850 mb

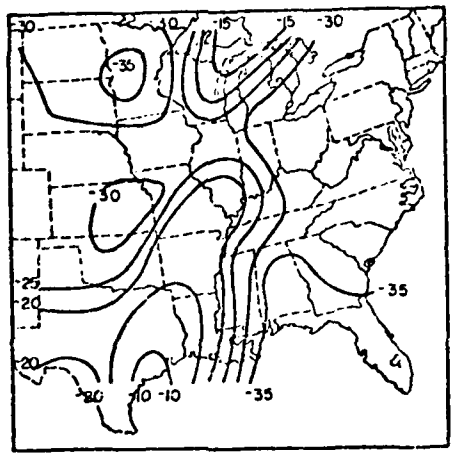

d. Rawinsonde (RW), 500 mb

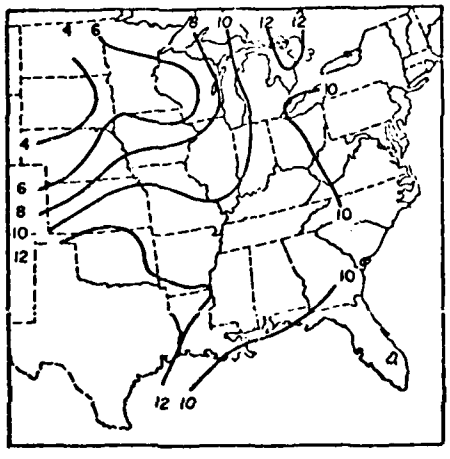

b. Satellite (S), 850 mb

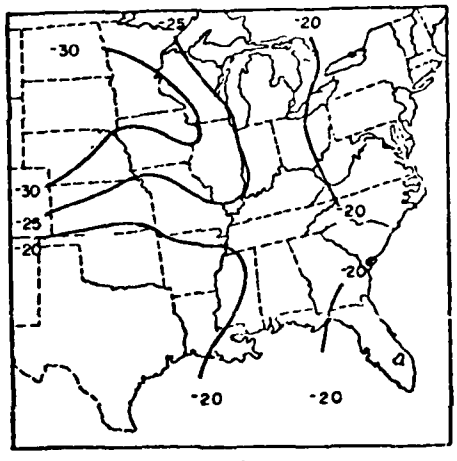

e. Satellite (S), 500 mb

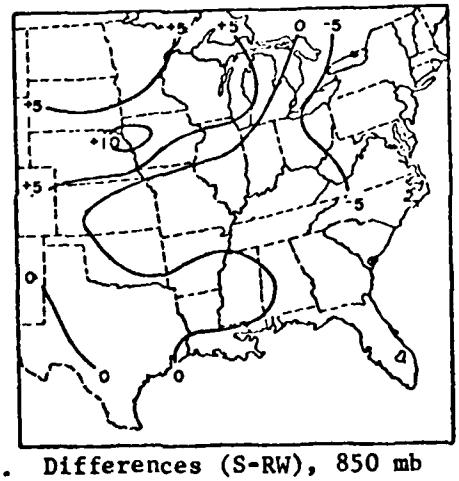

c. Differences (S-RW), 850 mb

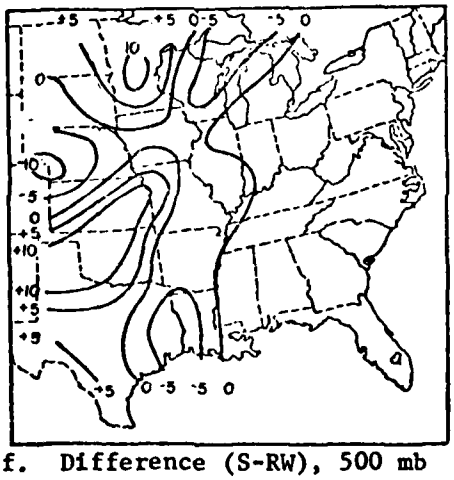

f. Difference (S-RW), 500 mb

Fig. 15. Charts of dew-point temperature and dew point difference (°C) at 850 and 500 mb for the central United States region (Area I).

since the gradient is quite strong in a band from Michigan to Colorado. Differences (Fig. 15c) are generally between 0°C and 5°C, although values of 10°C occur just behind the front. As with temperature, the front marks a line separating positive differences to the north from negative differences to the south.

The dew-point temperature map for rawinsonde data at 500 mb in Area I, also presented in Fig. 15, shows many areas of strong gradients of moisture which are not present in the satellite data. Maximum differences are located parallel to and just south of the front with values reaching 10°C. These differences do not correspond with cloudiness.

5.2 Cross Sections

The line of the cross section for Area I is shown in Fig. 6. Each figure of cross sections presented contains three parts: 1) a cross section derived from rawinsonde data; 2) a cross section derived from satellite data; and 3) a cross section of differences expressed as satellite minus rawinsonde values.

5.2.1 Temperature

The cross section of temperature for Area I (Fig. 16) shows the front in the northern part of the section to be relatively weak in terms of temperature contrast in the rawinsonde data, and weaker in the satellite data. This makes the front difficult to locate in the satellite cross section, but neither type of data locates the front except as being somewhere in a broad zone of baroclinity. The front was located by use of rawinsonde soundings, and the frontal position obtained also was used with the satellite data. One feature of the difference cross section is the presence of negative differences through most of the troposphere in the air south of the front. A layer of positive differences (satellite values too high) is present just under the tropopause in both air masses. These differences apparently are the result of vertical smoothing.

5.2.2 Moisture-related Variables

The cross section of rawinsonde dew point for Area I (Fig. 17) shows a moisture increase across the front from north to south associated with prefrontal shower activity, and fairly strong contrast across the front. The satellite section indicates much less contrast across the front with highly smoothed patterns. Differences are largest where the rawinsonde

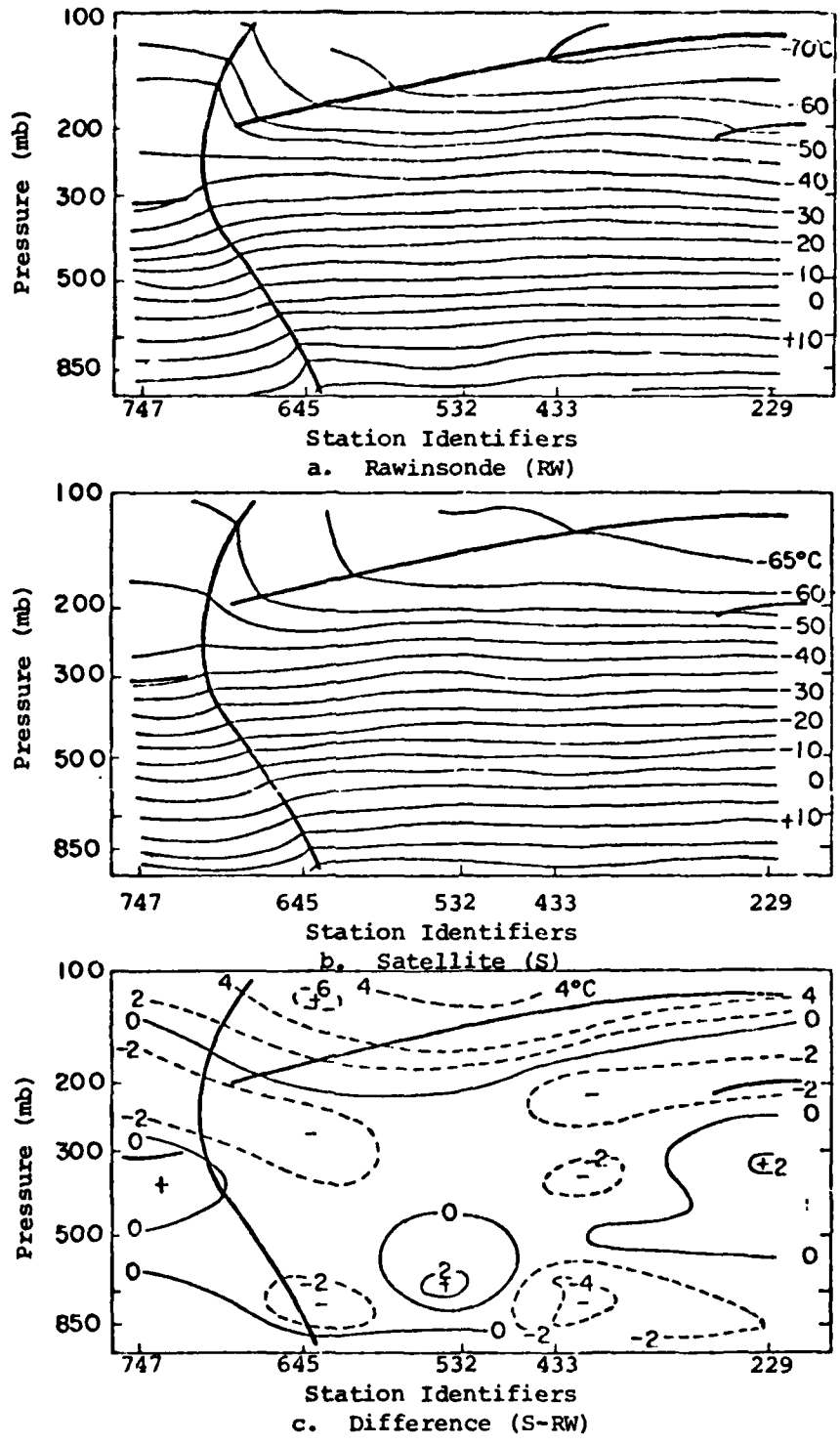

Fig. 16. Cross sections of temperature and temperature difference (°C) for the central United States region on 25 August 1975 at 1700 GMT. (See Fig. 6 for path of cross sections.)

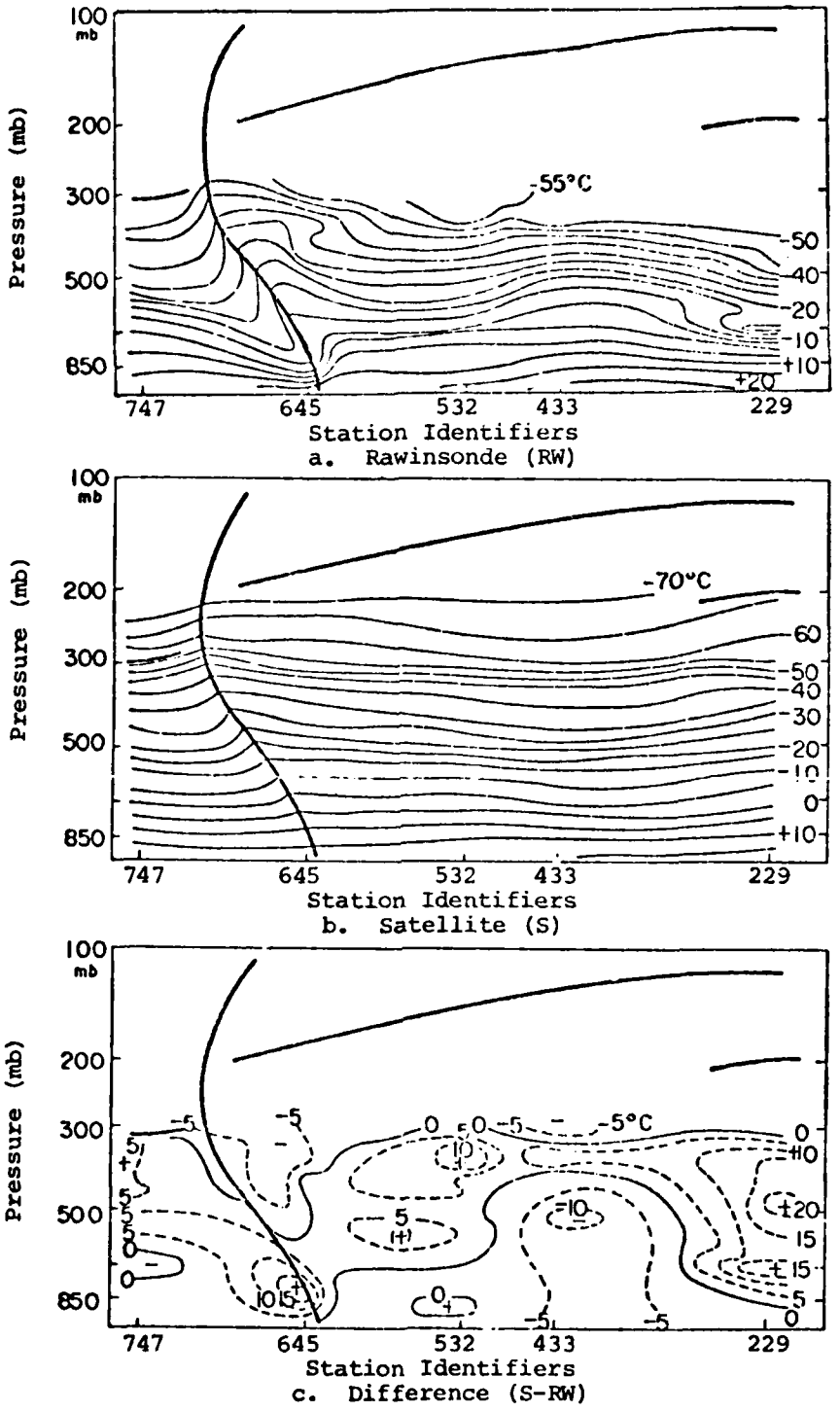

Fig. 17. Cross sections of dew-point temperature and dew point difference (°C) for the central United States region on 25 August 1975 at 1700 GMT. (See Fig. 6 for path of cross sections.)

gradients are largest. Without prior knowledge of the approximate location of the front, it would be difficult to locate the front on either the satellite cross section of temperature or dew-point temperature.

Cross sections of equivalent potential temperature for Area I are shown in Fig. 18. The difference in air mass structure and stability is shown in both types of data for this area. This appears to be a reliable variable to examine from satellite data for depiction of frontal contrasts between air masses. Differences in equivalent potential temperature measurements are largest near the surface where the largest differences in moisture measurement occur.

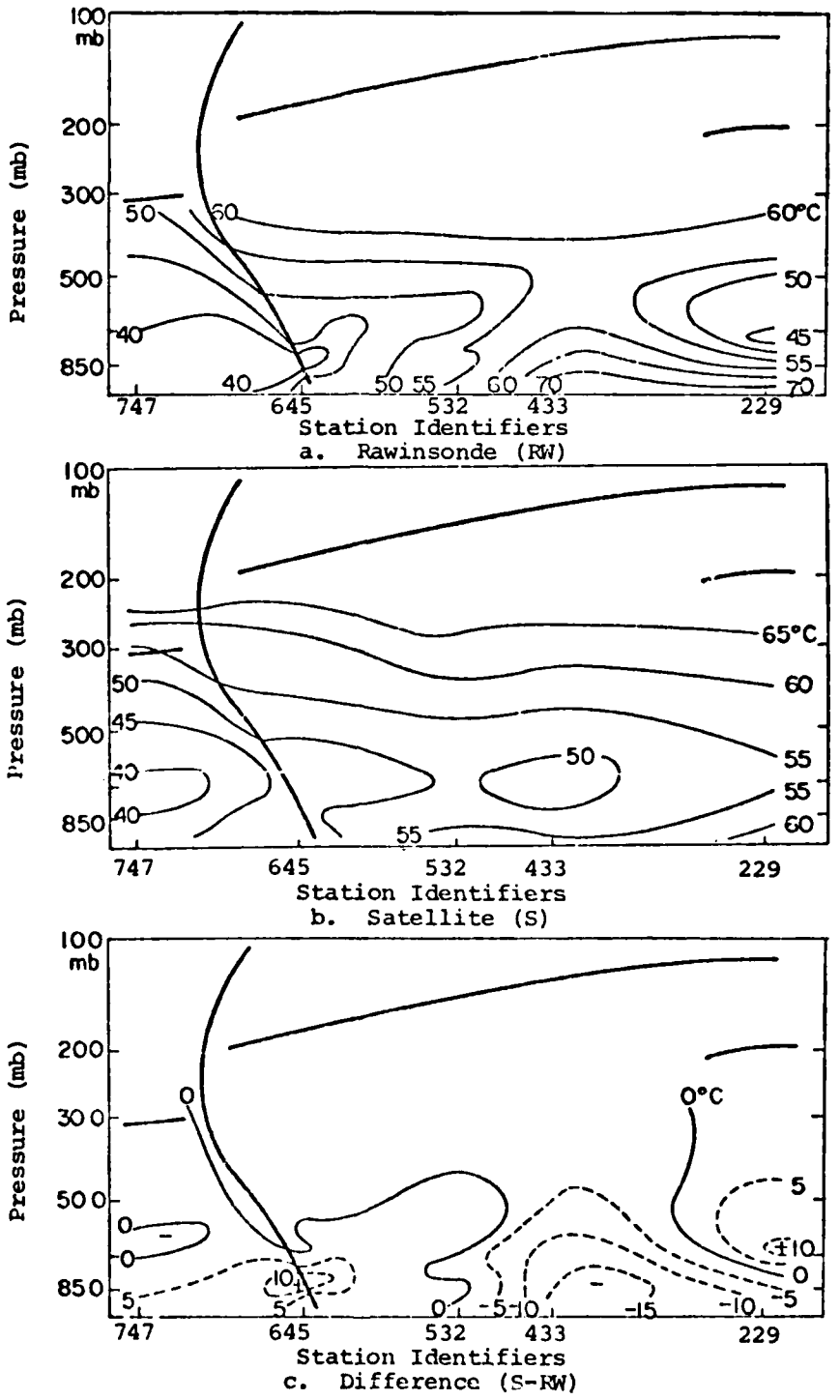

Fig. 18. Cross sections of equivalent potential temperature and equivalent potential temperature difference (°C) for the central United States region on 25 August 1975 at 1700 GMT. (See Fig. 6 for path of cross sections.)

6. DETERMINATION OF WIND FROM NIMBUS-6 SATELLITE SOUNDING DATA

Objective methods of computing upper-level and surface wind fields from Nimbus-6 satellite thermodynamic data were developed. Satellite-derived and rawinsonde wind fields are compared on gridded constant-pressure charts at nine pressure levels in Areas I-IV. Rawinsonde winds used in the comparisons are linearly interpolated to correspond in time to the satellite pass. Fields of satellite-derived surface wind are compared to fields of hourly-observed surface wind in three areas. Finally, rawinsonde and satellite-derived kinematic parameters are compared.

6.1 Satellite-Derived Winds on Constant-Pressure Surfaces

The best satellite-derived wind on constant-pressure surfaces is a geostrophic wind derived from highly smoothed fields of geopotential height. A nine-point smoothing routine (Shuman, 1957) was applied to the satellite-derived height fields over four grid distances with a smoothing parameter of 0.5. Effects of smoothing satellite-derived height fields before computing geostrophic wind fields are shown in Figs. 19 and 20. The differences between satellite geostrophic wind fields computed from smoothed fields of height and rawinsonde wind fields are shown by solid lines; similar differences resulting from unsmoothed satellite height fields are shown by dashed lines. Magnitudes of the average and standard deviation of the differences between satellite-derived geostrophic and rawinsonde wind speeds are decreased when satellite height fields are smoothed in most areas. Differences in wind direction were, in general, decreased by the smoothing process as shown in Fig. 20.

Average differences between geostrophic wind speed computed from smoothed fields of satellite-derived height and rawinsonde wind speed are generally positive in the middle and upper troposphere as shown in Fig. 19. Mean differences range from about -5 to 5 m s^{-1} and are smallest in Area II (Caribbean) where wind speeds are small at all levels. Magnitudes of the standard deviation of the differences in wind speed generally increase with altitude (decrease in pressure) until the level of the maximum rawinsonde wind speed is reached. At this level, magnitudes of the standard deviation are approximately 11, 5, 11, and 12 m s^{-1} in Areas I,

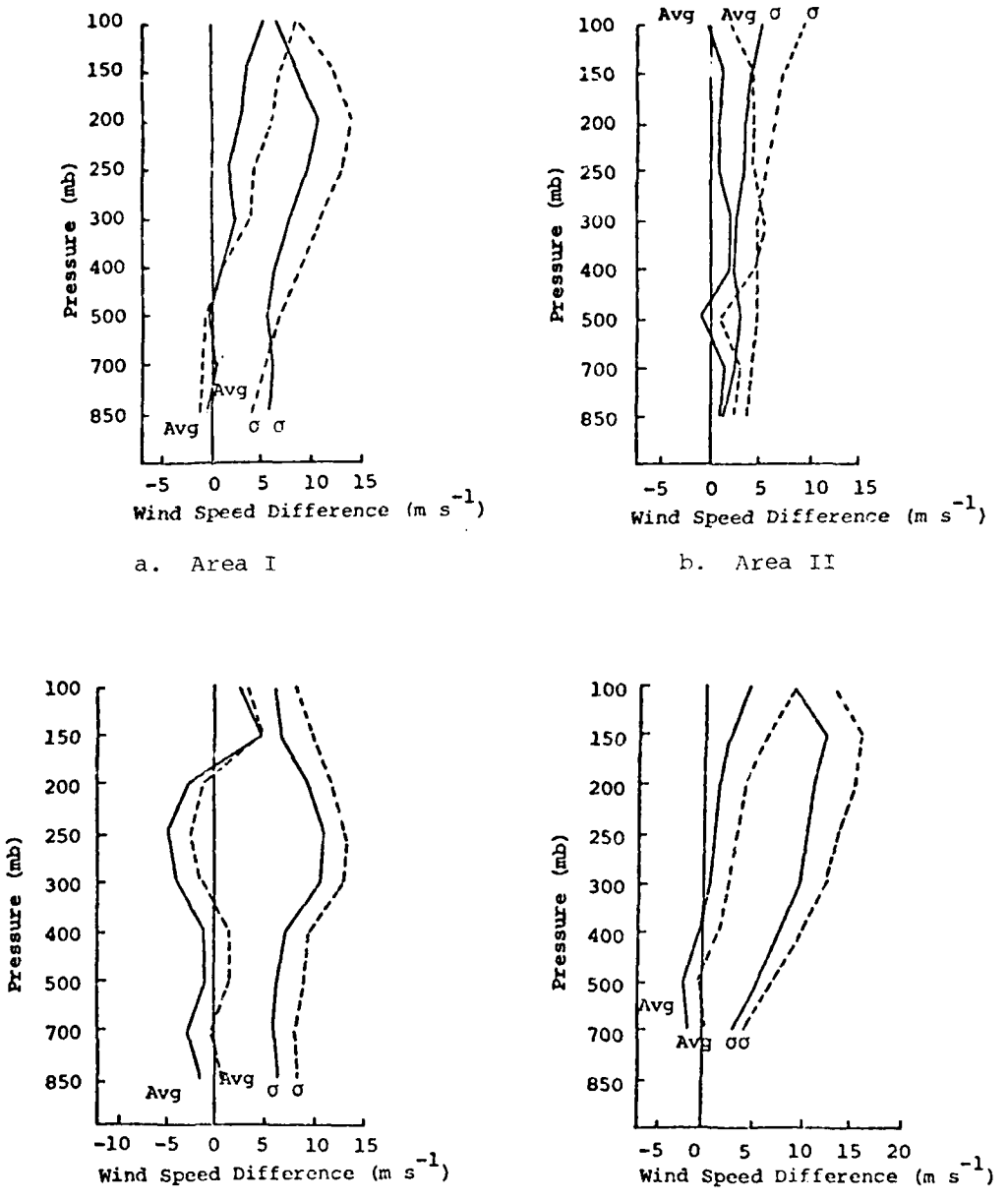

Fig. 19. Profiles of the average difference and standard deviation of the differences between satellite geostrophic wind speed computed from smoothed and unsmoothed heights and rawinsonde wind speed for Areas I-IV. Differences were computed by subtracting rawinsonde from satellite values.

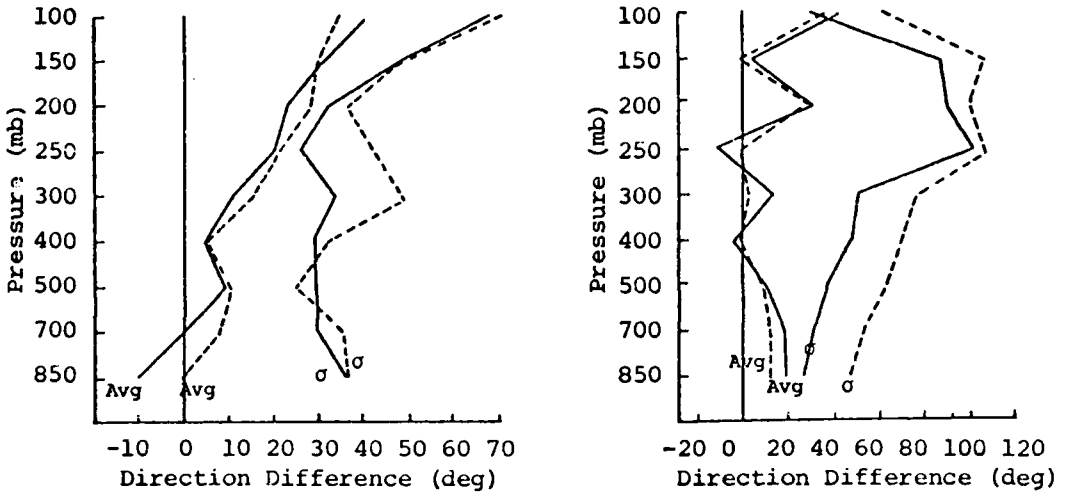

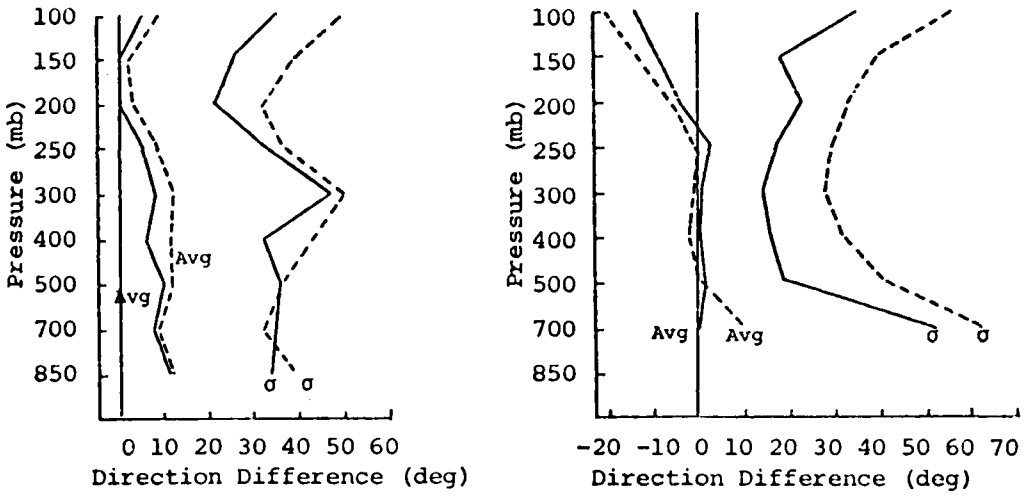

Fig. 20. Profiles of the average difference and standard deviation of the differences between satellite geostrophic wind direction computed from smoothed and unsmoothed heights and rawinsonde wind direction for Areas I-IV. Differences were computed by subtracting rawinsonde from satellite values.

II, III, and IV, respectively. The standard deviation of the differences in wind speed is between 3 and 12 m s^{-1} in Areas I, III, and IV, and varies from about 2 to 5 m s^{-1} in Area II.

Average differences and standard deviations of the differences between satellite geostrophic and rawinsonde wind directions, shown in Fig. 20, show the largest variation and generally large magnitudes in Area II where varying wind directions are associated with small wind speeds. Average differences in direction are between -12 and 41° in Area II and range from -14 to 40° in the other three areas. Magnitudes of the standard deviation of the differences in direction are between about 20 and 100° in Area II, and range from near 15 to 70° in the other three areas. Magnitudes of the standard deviation of the differences in direction are generally smallest near the level of maximum rawinsonde wind speed.

Satellite-derived and rawinsonde wind fields are presented in Fig. 21 for the 500-mb level for Area I. The two wind fields have similar flow patterns with centers of large differences in wind speed. Both fields of wind show anticyclonic flow and a wind-speed minimum in the southeastern portion of the area, and cyclonic flow and a wind speed maximum in the northern portion. The wind speed maximum from satellite data (approximately 45 m s^{-1}) is located northeast of the maximum from rawinsonde data (about 35 m s^{-1}). Thus, there are large positive differences between satellite-derived and rawinsonde wind speeds in this area.

Characteristics of the differences between satellite-derived and rawinsonde wind fields are as follows. Circulation patterns from satellite-derived geostrophic and rawinsonde wind fields are similar in regions of moderate to large wind speeds, but may compare poorly in regions of small wind speeds. Centers of maximum wind speed in satellite-derived wind fields may be displaced horizontally from the corresponding centers in rawinsonde data; a second maximum in wind speed may be present in satellite-derived winds where none exists in rawinsonde data. This also has been seen by other investigators (Arnold et al., 1976). Satellite-derived and rawinsonde winds show good agreement on the altitude of the jet stream core, but the jet core from satellite data has smaller wind speeds and less vertical shear of wind speed than are present in the rawinsonde jet core.

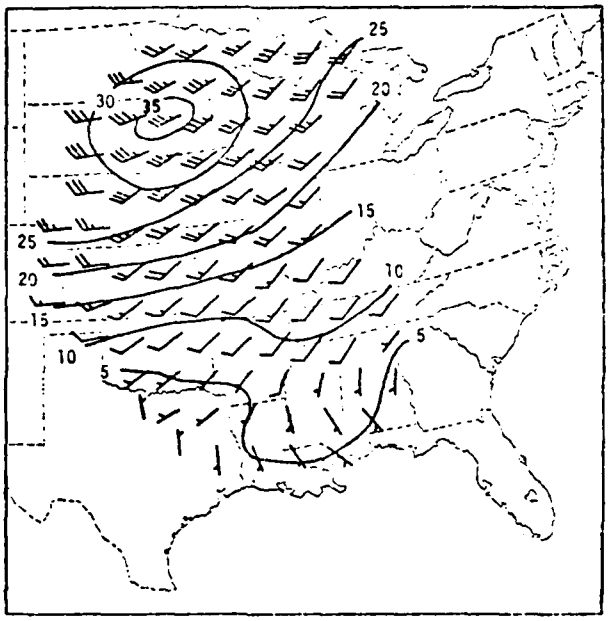

a. Rawinsonde

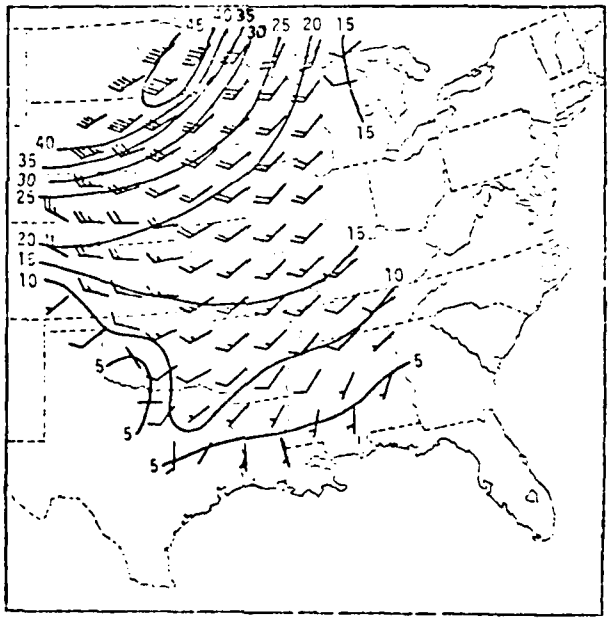

b. Satellite

Fig. 21. Plotted winds and isotach analyses (m s^{-1}) at 500 mb for the central United States region (Area I). Isotachs were drawn from exact values and barbs plotted to the nearest 5 m s^{-1}.

Use of the gradient wind approximation did not improve comparisons between satellite-derived and rawinsonde wind speeds. This is because the differences between satellite geostrophic and rawinsonde wind speeds do not correspond to the curvature of the satellite-derived contours. Areas of large positive and negative differences between satellite-derived geostrophic and rawinsonde wind speeds are not associated with troughs, ridges, or any other large-scale pattern.

6.2 Satellite-derived Surface Wind

Wind speed and direction through the boundary layer to the surface were computed from gridded fields of geopotential height. The u and v components of wind were assumed to vary linearly with height above 150 m to the first level of data, and wind speed was assumed to have a logarithmic profile below 150 m. Wind direction at a grid point was assumed to be constant through the boundary layer. Surface wind speed, V_s, was computed according to

$$V_s = \left(\frac{\ln Z_s - \ln Z_o}{\ln Z_r - \ln Z_o}\right) \cdot V_r$$

where Z_s is the height of the surface wind, Z_o is roughness length, and Z_r is a reference height at which a value for wind speed (V_r) is known.

Surface wind speed was computed for a height of 10 m. A value of 0.5 m was used for roughness length in Areas I and III, and a value of 0.2 m was used in Area II. These values are in agreement with values presented by Fiedler and Panofsky (1972) and Garratt (1977). Fields of satellite-derived geostrophic wind were used to define a reference wind speed and direction at each grid point.

Average differences and standard deviations of the differences between satellite-derived and hourly-observed surface winds are presented in Table 6 for Area I (central U.S.), Area II (Caribbean), and Area III (Canada). The average difference and the standard deviation of the differences between satellite-derived and observed surface wind speeds are smallest in the central United States where observed wind speeds were generally between 3 and 8 m s^{-1}. The large standard deviation of the differences in wind speed in Canada may be associated with the large

Table 6. Average differences and standard deviations of the differences between satellite-derived (S) and hourly-observed (O) surface winds (S-O) for three regions.

Region	Speed ($m\ s^{-1}$)		Direction (deg)	
	Avg.	Std. Dev.	Avg.	Std. Dev.
Central United States	-0.3	2.1	16	34
Caribbean	1.5	2.8	21	66
Canada	0.9	4.3	30	28

wind speeds and the intense low-pressure center in the area. The differences between satellite-derived and observed wind speeds in the Caribbean are larger than expected in this region of very low wind speeds.

The magnitude of the standard deviation of the differences in wind direction is largest in the Caribbean where surface winds were light and variable. The magnitude of the standard deviation of the differences in surface wind direction is smallest in Canada where the satellite-derived flow pattern is similar to the well-organized observed flow pattern.

Fields of satellite-derived and observed surface winds are presented in Fig. 22 for Area I. Both fields of wind indicate anticyclonic flow in the southeastern portion of the region, weak cyclonic flow in the northern portion, and strong cyclonic flow around the surface low-pressure center in Oklahoma. Magnitudes of the differences in wind speed are less than 3 $m\ s^{-1}$ at most grid points. Observed surface winds accelerate as they cross the isobars toward lower pressure. This acceleration was not taken into account in the computation of satellite-derived surface wind speeds and leads to negative differences in wind speed (satellite values too small) near Oklahoma and the Great Lakes.

6.3 Comparisons of Satellite and Rawinsonde-derived Kinematic Parameters

Kinematic parameters were computed from gridded fields of rawinsonde and satellite data for Areas I-IV. Horizontal advection of temperature, the vertical component of relative vorticity, and the horizontal advection of absolute vorticity were computed. The rawinsonde calculations used fields of temperature and wind from rawinsonde measurements, while the

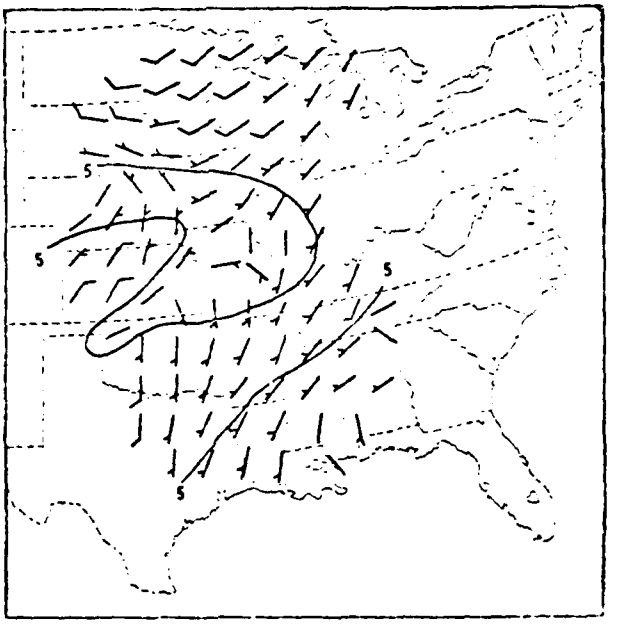

a. Observed

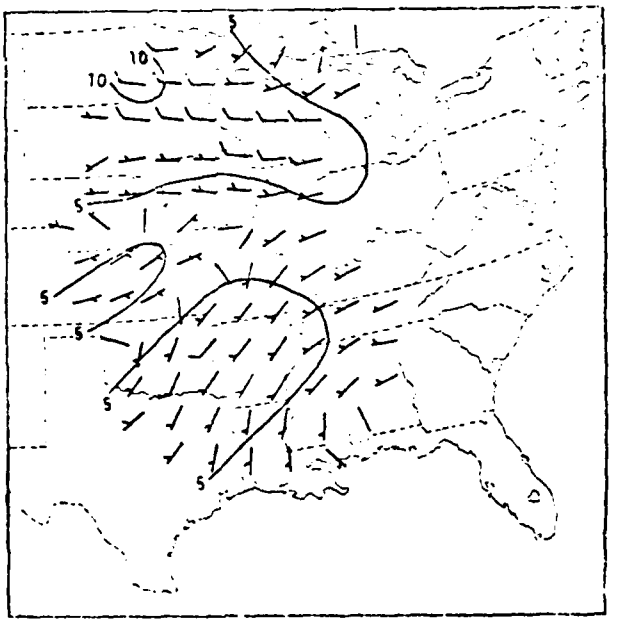

b. Satellite

Fig. 22. Plotted surface wind and isotach analyses (m s^{-1}) for the central United States region (Area I).

satellite calculations used fields of temperature and geostrophic wind from satellite data.

Rawinsonde and satellite-derived fields of temperature advection are similar at 850 and 500 mb. As shown in Fig. 23, rawinsonde and satellite-derived fields of temperature advection at 850 mb indicate cold-air advection over northern Wisconsin and warm-air advection over northeastern Oklahoma. Magnitudes of warm-air advection are nearly the same for both types of data, while satellite-derived magnitudes of cold-air advection over Wisconsin are smaller than the rawinsonde values. Fields of horizontal advection of temperature for Areas II-IV (not shown) indicate that satellite data are capable of depicting centers of positive and negative temperature advection for each of the synoptic conditions considered in this study.

There is little correspondence between the rawinsonde and satellite-derived fields of relative vorticity at 500 mb. Centers of relative vorticity from the two data sets are generally of opposite sign in Areas I, II, and IV. Fields of relative vorticity computed from the two types of data are similar only in Canada where the 500-mb flow was strong and cyclonic. Fields of satellite-derived advection of absolute vorticity at 500 mb are dissimilar to corresponding rawinsonde fields in each of the four areas.

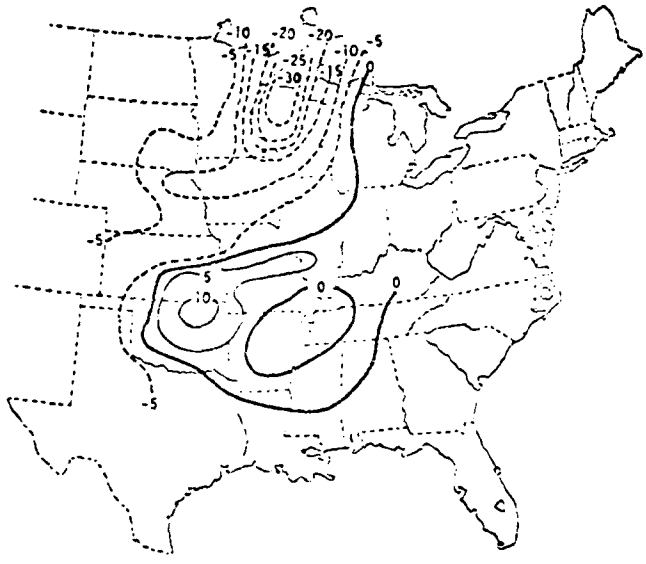

a. Rawinsonde

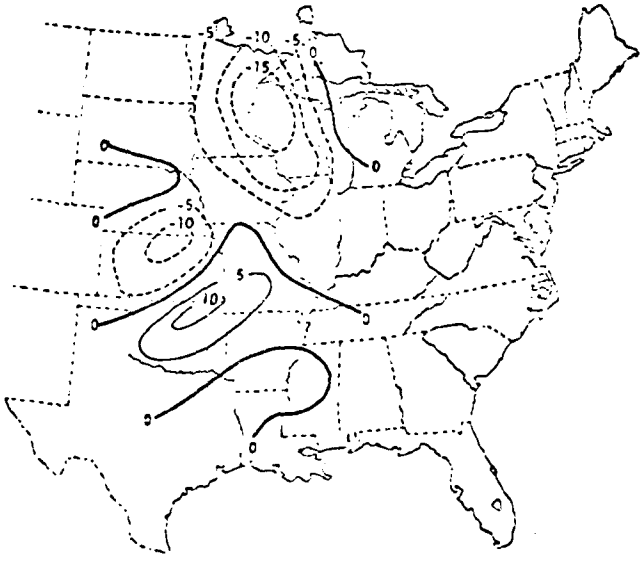

b. Satellite

Fig. 23. Fields of horizontal advection of temperature (10^{-6} °C s^{-1}) at 850 mb for the central United States region (Area I).

7. COMPARISONS BETWEEN SIMULTANEOUS TIROS-N AND RAWINSONDE DATA FOR 2100 GMT ON 10 APRIL 1979

The analysis of atmospheric structure determined from quantitative satellite data has been extended to include a case with simultaneous rawinsonde and TIROS-N sounding data. This research has two objectives. The first objective is to determine the limitations of TIROS-N sounding data for the purpose of determining the atmospheric structure in a meteorologically active area. The second objective of this research is to aid in the evaluation of the results obtained for Areas I-VII with Nimbus-6 and time-interpolated rawinsonde data. Simultaneous TIROS-N and rawinsonde soundings provide an opportunity to compare satellite and rawinsonde data without the risk of incurring errors from a time-interpolation process.

Except for the lack of a time-interpolation process, all procedures used in the analysis of data in the AVE-SESAME area are identical to those followed for Areas I-VII. Satellite data, rawinsonde data, and synoptic conditions for the AVE-SESAME area were described in Section 2.

7.1 Analysis of Discrepancies Between Rawinsonde and TIROS-N Profile Parameters

For the purpose of comparison, TIROS-N soundings were paired with the closest rawinsonde soundings. Not all satellite data were used since there were more satellite than rawinsonde soundings. The 20 pairings of satellite sounding locations and rawinsonde stations are shown in Fig. 24.

Seven parameters were considered in this study: temperature, dew-point temperature, mixing ratio, thickness, lapse rate of temperature, precipitable water, and stability. Discrepancies between satellite and rawinsonde data for all seven parameters were computed by subtracting rawinsonde from satellite values and were analyzed in the same manner as those obtained for Areas I-VII.

7.1.1 Temperature

Table 7 shows the mean and standard deviation of the mean discrepancy, the absolute mean discrepancy, and the root-mean-square discrepancy (RMSD) between TIROS-N and rawinsonde temperatures. The statistics were obtained from the lumped discrepancies for all levels reported from each station in

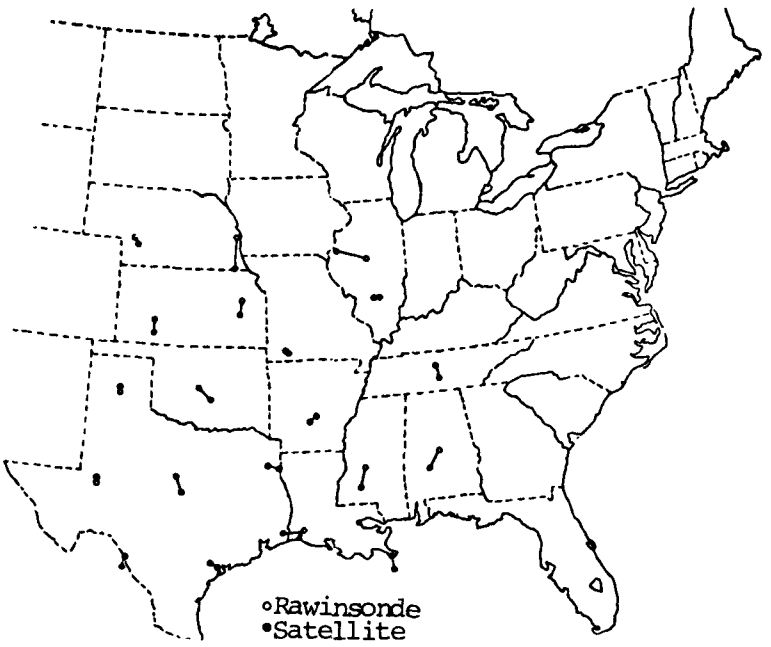

Fig. 24. Pairings of satellite sounding locations and rawinsonde stations at 2100 GMT on 10 April 1979.

The region to provide a single set of criteria by which to judge the results of the comparisons. The mean discrepancy of -0.5°C is of opposite sign of those found in previous areas (see Table 2). This indicates TIROS-N-derived temperatures contain a negative bias relative to rawinsonde-derived temperatures. The mean RMSD of 1.8°C is smaller than that found in most of the previous areas (Table 2).

The means and standard deviations of temperature discrepancies for

Table 7. Mean ($\bar{x}$) and standard deviation (σ), lumped for all levels reported for each station and for all stations in the SESAME region, of the mean discrepancy ($\bar{\delta}$), the absolute mean discrepancy ($|\bar{\delta}|$), and the root-mean-square discrepancy (RMSD), in degrees Celsius, between TIROS-N and rawinsonde temperatures and dew points [$\delta \equiv (T_S - T_R)$].

	Temperature			Dew-Point Temperature			Station Pairs
	$\bar{\delta}$	$\lvert\bar{\delta}\rvert$	RMSD	$\bar{\delta}$	$\lvert\bar{\delta}\rvert$	RMSD	
$\bar{x}$	-0.5	1.5	1.8	-2.7	9.4	10.9	20
σ	0.5	0.4	0.5	8.4	4.2	4.3	

all three layers are shown in Table 8, and the cumulative frequency distributions plotted on probability paper are shown in Fig. 25.

Table 8. Means and standard deviations of discrepancies (S-R) between TIROS-N and rawinsonde data for selected parameters by layer for the SESAME region at 2100 GMT on 10 April 1979.

		1000-500 mb	500-300 mb	300-100 mb
Temperature (°C)	Mean	-0.8	0.4	-0.6
	Standard deviation	1.8	1.5	1.8
	No. of data points	63	60	96
Dew point (°C)	Mean	-3.3	-2.3	-
	Standard deviation	9.1	12.9	-
	No. of data points	63	60	-
Lapse rate (°C/km)	Mean	-0.3	-0.1	0.3
	Standard deviation	0.5	0.7	0.8
	No. of data points	43	59	76
Mixing ratio (gm/kgm)	Mean	-0.9	0.0	-
	Standard deviation	2.0	0.5	-
	No. of data points	63	60	-
Precipitable water (mm)	Mean		-1.2	
	Standard deviation		2.3	
	No. paired profiles		20	

The mean discrepancies listed in Table 8 indicate that there is a negative bias between the satellite and rawinsonde temperature data in the 1000 to 500- and 300 to 100-mb layers. The negative bias in satellite-derived temperatures for the 300 to 100-mb layer was not present in any of the areas previously studied (see Table 3) and is partially responsible for the negative mean discrepancy for the lumped data (Table 7). Magnitudes of the standard deviation of temperature discrepancies range from 1.5°C in the middle layer to 1.8°C in the upper and lower layers and are similar to those found in the first central United States case (Area I). Except for

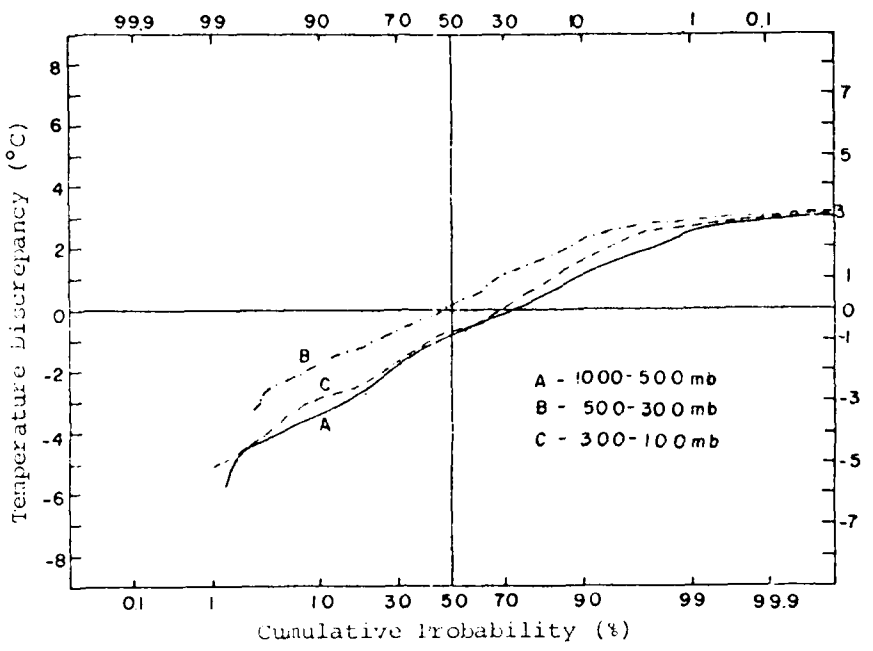

Fig. 25. Cumulative probability frequency distributions of temperature discrepancies within the layers 1000 to 500 mb, 500 to 300 mb, and 300 to 100 mb for the AVE-SESAME area.

the second Canada and Caribbean areas, the standard deviation of temperature discrepancies is smallest in the middle layer for all areas studied.

The cumulative frequency distributions shown in Fig. 25 are approximately normal (straight lines) except near the extremes. The small sample size is inadequate for defining the extremes of the distributions. The tendency for the cumulative frequency distributions to be straight lines when plotted on probability paper suggests that the discrepancies between TIROS-N and rawinsonde temperatures are due to random errors.

7.1.2 Dew-point Temperature

Statistics for the ensemble of discrepancies between satellite and rawinsonde dew-point temperatures also are shown in Table 7. TIROS-N soundings of dew-point temperature are not as reliable as those of temperature. The mean RMS discrepancy for the SESAME area, 10.9°C, is larger than those found in all but one of the areas previously studied.

Discrepancies in dew-point temperature were examined for the 1000 to 500- and 500 to 300-mb layers. Means and standard deviations of the discrepancies within the two layers are shown in Table 8, and cumulative frequency distributions are shown in Fig. 26. The mean difference is smaller in the higher layer than in the lower layer, a result opposite of those found in all areas studied previously, except for the second Canadian area. The standard deviation of the discrepancies in dew-point temperature are smaller in the lower layer than in the upper layer. This agrees with the results found in most of the previous areas. The plotted cumulative frequency distributions for dew-point temperature discrepancies (Fig. 26) are not as straight as those for temperature discrepancies (Fig. 25), but may be considered as straight lines as a first approximation.

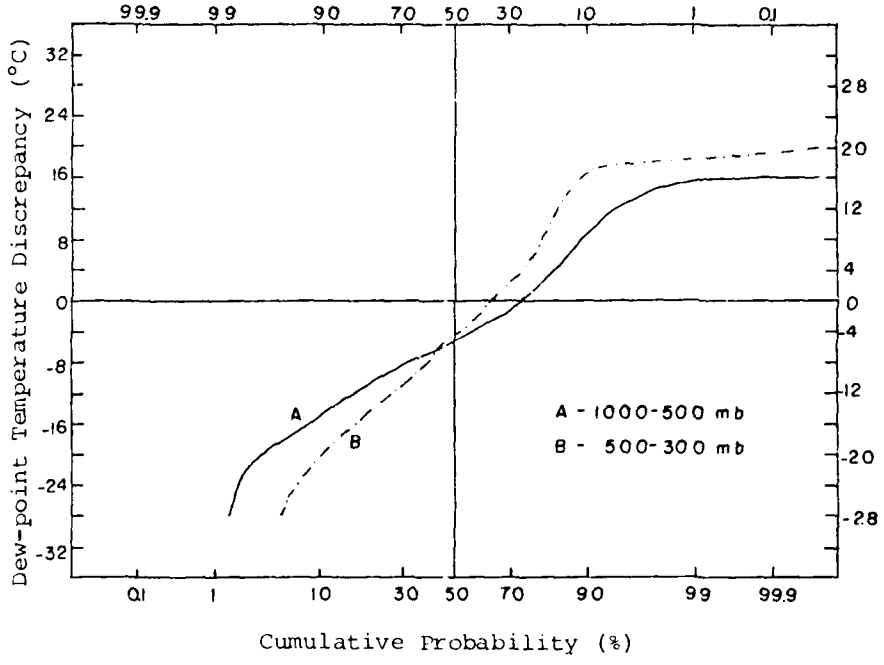

Fig. 26. Cumulative probability frequency distributions of dew-point temperature discrepancies within the layers 1000 to 500 mb and 500 to 300 mb for the AVE-SESAME area.

7.1.3 Thickness

Layer thickness discrepancies, normalized to units of m km^{-1}, were stratified into three layers. Means and standard deviations of thickness discrepancies are presented in Table 9. Values of the standard deviation of discrepancies range from 4.7 to 6.3 m km^{-1} and increase with altitude. Cumulative probability curves for normalized discrepancies in thickness (not shown) are approximately straight lines.

Table 9. Means and standard deviations of normalized discrepancies in thickness for the layers 1000 to 500 mb (A), 500 to 300 mb (B), and 300 to 100 mb (C) for the AVE-SESAME area (m km^{-1}).

	A	B	C
Mean	-3.1	0.3	-1.9
St. Dev.	4.7	5.4	6.3
No. of Data	43	60	96

7.1.4 Mixing Ratio

Mixing ratio values were obtained from dew-point temperature data plotted on skew T-log p diagrams for rawinsonde and TIROS-N soundings. The results of comparisons between satellite and rawinsonde-derived mixing ratios are presented in Table 8. The mean and standard deviation of the discrepancies in the lower layer are greater than those found in the upper layer for the AVE-SESAME area. These results are in agreement with those found for all previous areas studied (Table 3). Magnitudes of the standard deviation of the discrepancies in mixing ratio are 2.0 and 0.5 g kg^{-1} for the lower and upper layers, respectively. These values are similar to those found in the other areas.

7.1.5 Precipitable Water

The mean and standard deviation of the discrepancies in precipitable water are presented in Table 8. The results indicate that TIROS-N soundings yield values of precipitable water which are smaller than those from rawinsonde data. The standard deviation of 2.3 mm is of approximately the same magnitude as those found in the other areas (see Table 3).

7.1.6 Lapse Rate of Temperature

Lapse rates computed from satellite and rawinsonde data were normalized to units of °C km^{-1}. Discrepancies in lapse rate were stratified into three layers: 1000 to 500 mb, 500 to 300 mb, and 300 to 100 mb.

Results shown in Table 8 indicate that satellite-derived lapse rates have a negative bias in the lower two layers and a positive bias in the upper layer. Magnitudes of the standard deviation of the discrepancies range from 0.5 to 0.8°C km^{-1} and are generally smaller than those found in previous areas (Table 2). When comparing normalized results from the SESAME area with those from previous areas, the depth of the layer through which the lapse rate is computed must be considered. Because soundings for the first four areas contained 21 levels of data and for the AVE-SESAME area only 10 levels, results can not be strictly compared. Results from Areas V-VII may be compared with those from the present study since soundings for these areas also contained 10 levels of data. Magnitudes of the standard deviation of discrepancies in lapse rate are smaller and have a smaller range in the AVE-SESAME area than in Areas V-VII.

7.1.7 Stability

Showalter and Vertical Totals indexes computed from TIROS-N and rawinsonde data and the discrepancy for each station pair are shown in Tables 10 and 11, respectively. The mean and standard deviation of the discrepancies also are presented for each index.

All Showalter Indexes computed from satellite data were positive; this also was true in each of the other areas studied. Smaller percentage errors in the mean and standard deviation of discrepancies were found for the vertical totals index than for the Showalter index. The mean and standard deviation of discrepancies are 4.1 and 4.6 for the Showalter index, and -0.9 and 2.2 for the vertical totals index. These results are similar to those found for Areas I-IV.

7.2 Analysis of Discrepancies Between Rawinsonde and TIROS-N Data on Constant-Pressure Surfaces

7.2.1 Temperature

Profiles of the average and standard deviation of differences in temperature are shown in Fig. 27. The average difference increases from

Table 10. Discrepancies in the Showalter Index derived from TIROS-N and rawinsonde data for the AVE-SESAME area.

Station No.	Satellite	Rawinsonde	Discrepancy
353	6.6	-2.9	9.5
553	8.9	7.3	1.6
532	13.8	15.5	-1.7
433	13.1	15.3	-2.2
260	1.8	-4.3	6.1
456	7.3	3.0	4.3
255	0.5	-4.5	5.0
363	4.7	3.6	1.1
232	4.4	4.4	0.0
229	7.8	-0.8	8.6
261	7.6	-3.9	11.5
451	2.0	2.1	-0.1
235	5.8	-2.3	8.1
240	7.0	-0.2	7.2
340	6.6	-2.0	8.6
247	0.3	-2.6	2.9
265	6.8	1.0	5.8
349	9.0	-1.2	10.2
327	7.5	11.7	-4.2
562	9.2	10.3	-1.1
Mean	4.1		
Standard Deviation	4.6		

Table 11. Discrepancies in the Vertical Totals Index derived from TIROS-N and rawinsonde data for the AVE-SESAME area.

Station No.	Satellite	Rawinsonde	Discrepancy
353	24.7	27.3	-2.6
553	23.8	23.3	0.5
532	21.0	18.0	3.0
433	22.4	23.5	-1.1
260	27.3	27.9	-0.6
456	24.8	24.9	-0.1
255	25.7	26.9	-1.2
363	28.6	28.4	0.2
232	22.2	24.4	-2.2
229	25.2	25.3	-0.1
261	30.4	31.4	-1.0
451	27.7	30.0	-2.3
235	23.7	26.6	-2.9
240	24.4	28.8	-4.4
340	24.0	26.3	-2.3
247	28.0	27.0	1.0
265	31.7	36.4	-4.7
349	24.4	26.9	-2.5
327	26.6	24.9	1.7
562	23.5	19.5	4.0
Mean	-0.9		
Standard Deviation	2.2		

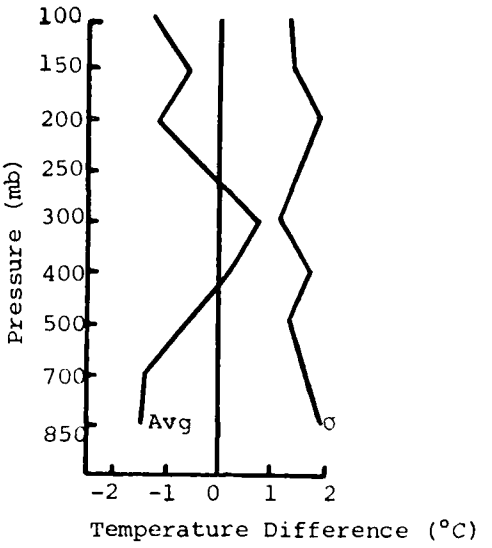

Fig. 27. Profiles of average and standard deviation of differences between satellite and rawinsonde temperatures (satellite minus rawinsonde) for the AVE-SESAME area.

approximately -1.5°C at 850 mb to nearly 0.7°C at 300 mb, then decreases to -1.3°C at 100 mb. The maximum standard deviation of the differences is about 1.9°C and occurs at 850 and 200 mb. The standard deviation is about 1.2°C at 500, 300, and 100 mb. Results from previous areas also indicated that relatively large magnitudes of the standard deviation occur near the tropopause and the ground. Comparison of results shown in Table 12 with those for previous areas (Table 5) indicates that the magnitude of the standard deviations of differences between TIROS-N and simultaneous rawinsonde temperatures are similar to those between Nimbus-6 and time-interpolated rawinsonde temperatures.

7.2.2 Dew-point Temperature

Profiles of the average and standard deviation of the differences between TIROS-N and rawinsonde dew-point temperatures are shown in Fig. 28. The average difference is negative at all levels which indicates that satellite dew-points are, on the average, lower than rawinsonde values. The standard deviation of the differences ranges from about 5 to 10°C and is considerably larger than the corresponding values for temperature presented in Fig. 27. Comparison with past results for dew-point temperature indicates that the average difference generally is of opposite sign to those obtained in previous areas and the standard deviation is larger for the AVE-SESAME area.

Table 12. Means and standard deviations of discrepancies between gridded satellite and rawinsonde parameters on selected constant pressure surfaces for the AVE-SESAME area at 2100 GMT on 10 April 1979.

		700 mb	500 mb	300 mb
Temperature (°C)	Mean	-1.4	-0.6	0.7
	Standard Deviation	1.6	1.3	1.2
	Approx. Magnitude	-3/10	-18	-40/-48
Dew-point Temperature (°C)	Mean	-3.8	-5.4	-6.3
	Standard Deviation	10.2	5.4	9.9
	Approx. Magnitude	-2/-20	-20/-36	-52
Lapse Rate of Temperature (°C/km)	Mean	-0.2	-0.3	0.1
	Standard Deviation	0.5	0.3	0.8
	Approx. Magnitude	4.5/8.0	7.5	7.2
Magnitude of Horizontal Gradient of Temperature (°C/1000 km)	Mean	0.3	2.1	0.0
	Standard Deviation	4.3	3.2	5.1
	Approx. Magnitude	1/25	1/15	1/13
Geopotential Height (m)	Mean	-19.2	-32.3	-27.8
	Standard Deviation	18.2	27.0	42.6
	Approx. Magnitude	3000	5600	9300
Geo. u-comp. Wind (m/s)	Mean	-0.7	0.9	3.9
	Standard Deviation	5.4	7.0	10.9
	Approx. Magnitude	-6/30	-2/40	-7/50
Geo. v-comp. Wind (m/s)	Mean	2.5	4.0	6.0
	Standard Deviation	4.5	7.0	11.1
	Approx. Magnitude	4/26	5/36	10/50
Scalar Wind Speed (m/s)	Mean	2.9	4.6	8.1
	Standard Deviation	4.1	7.0	11.5
	Approx. Magnitude	10/30	15/50	15/70
Wind Direction (deg)	Mean	-8.7	-4.8	-1.7
	Standard Deviation	20.2	17.6	17.0
	Approx. Magnitude	200	210	230
No. of data points			95	

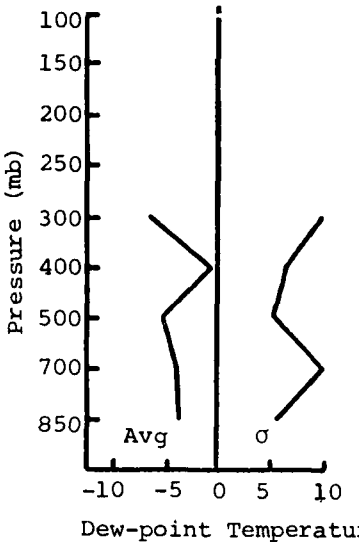

Fig. 28. Profiles of average and standard deviation of differences between satellite and rawinsonde dew-point temperatures (satellite minus rawinsonde) for the AVE-SESAME area.

7.2.3 Lapse Rate and Horizontal Gradient of Temperature

Profiles of the average and standard deviation of differences in lapse rates are shown in Fig. 29. The average difference curve shows that lapse rates from TIROS-N data are smaller than those from rawinsonde data at levels below 300 mb and are larger above 300 mb. Average differences vary from about -0.4 to 0.7°C km^{-1} which is a larger range than was found in previous areas. The standard deviation ranges from nearly 0.3 to 0.9°C km^{-1} with a maximum magnitude at 250 mb.

Vertical difference profiles for the horizontal gradient of temperature are shown in Fig. 30. The average difference varies from about -2 to 2°C $(1000\ km)^{-1}$ with gradients from satellite data being larger on constant-pressure surfaces between 700 and 300 mb and above 200 mb. Magnitudes of the standard deviation range from approximately 3.2 to 6.5°C $(1000\ km)^{-1}$ and are similar to those found in the first central United States area.

7.2.4 Geopotential Height

Vertical difference profiles for geopotential height are shown in Fig. 31. Average differences decrease from about -7 m at 850 mb to nearly -38 m at 100 mb, indicating that satellite-derived geopotential heights

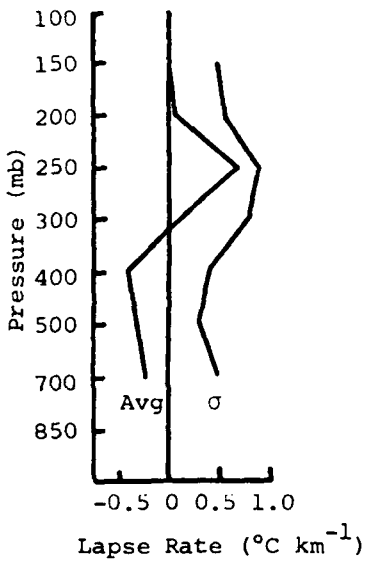

Fig. 29. Profiles of average and standard deviation of differences between satellite and rawinsonde vertical lapse rates for the AVE-SESAME area.

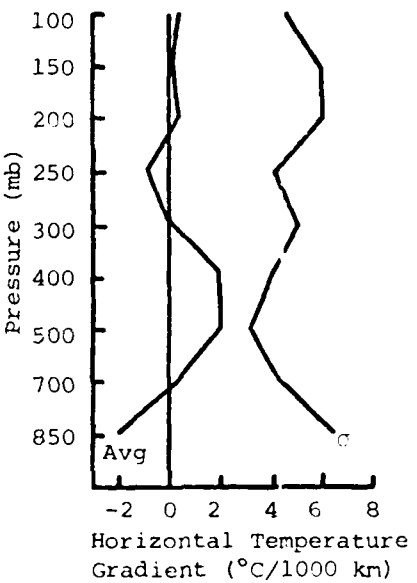

Fig. 30. Profiles of average and standard deviation of differences between satellite and rawinsonde horizontal temperature gradients for the AVE-SESAME area.

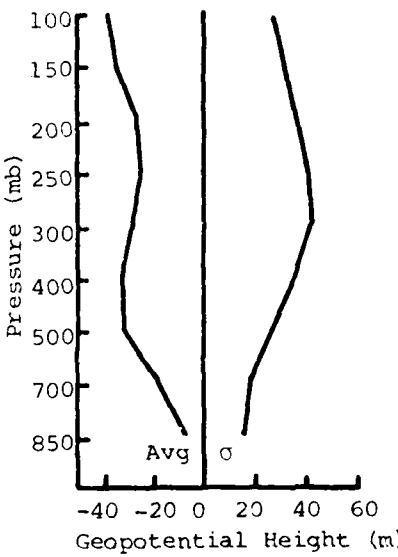

Fig. 31. Profiles of average and standard deviation of differences between satellite and rawinsonde geopotential heights for the AVE-SESAME area.

are smaller, on the average, than those from rawinsonde data at all levels. This is due to the negative bias in TIROS-N temperatures and dew-point temperatures relative to rawinsonde data. Magnitudes of the standard deviation increase from nearly 16 m at 850 mb to about 43 m at 300 mb, then decrease to approximately 29 m at 100 mb. The range in the standard deviation is similar to those found in other areas.

7.2.5 Geostrophic Wind

Profiles of the differences between geostrophic winds computed from rawinsonde and TIROS-N geopotential heights are presented in Fig. 32 for the u and v component wind speeds, scalar wind speed, and wind direction. Average differences between the component wind speeds are less than 6 m s^{-1} at all altitudes and are generally positive. Magnitudes of the standard deviation of the differences in component wind speeds range from about 4 to 14 m s^{-1} and are largest near the level of the tropopause. Average differences between geostrophic scalar wind speeds range from about 3 to 8 m s^{-1}, indicating that geostrophic wind speeds computed from satellite-derived height fields are larger, on the average, than those from rawinsonde data at all levels. Standard deviations increase from about 3.5 m s^{-1} at 850 mb to 13.0 m s^{-1} at 250 mb, then decrease to nearly 10.5 m s^{-1} at 100 mb. Magnitudes of the average difference in wind direction are less than 10° at all levels, while the standard deviation of the differences in direction ranges from about 16 to 28°.

Comparison of these results with those from previous areas shows that differences in component and scalar wind speeds in the AVE-SESAME area are similar to those in other areas. However, the magnitude and range of the average and standard deviation of the differences in geostrophic wind direction are significantly smaller in the AVE-SESAME area. Mean differences and standard deviations of the differences in wind direction ranged from about -30 to 0° and 30 to 80°, respectively, in the first central United States area. The improved results for geostrophic wind direction in the present area probably are due to the synoptic conditions in the area or the use of simultaneous rawinsonde and satellite data.

Profiles of the differences between observed wind and satellite-derived geostrophic wind are presented in Fig. 33. Average differences between the component wind speeds range from about -2 to 7 m s^{-1}, while the standard deviations vary from about 4 to 14 m s^{-1}. Average differences in scalar

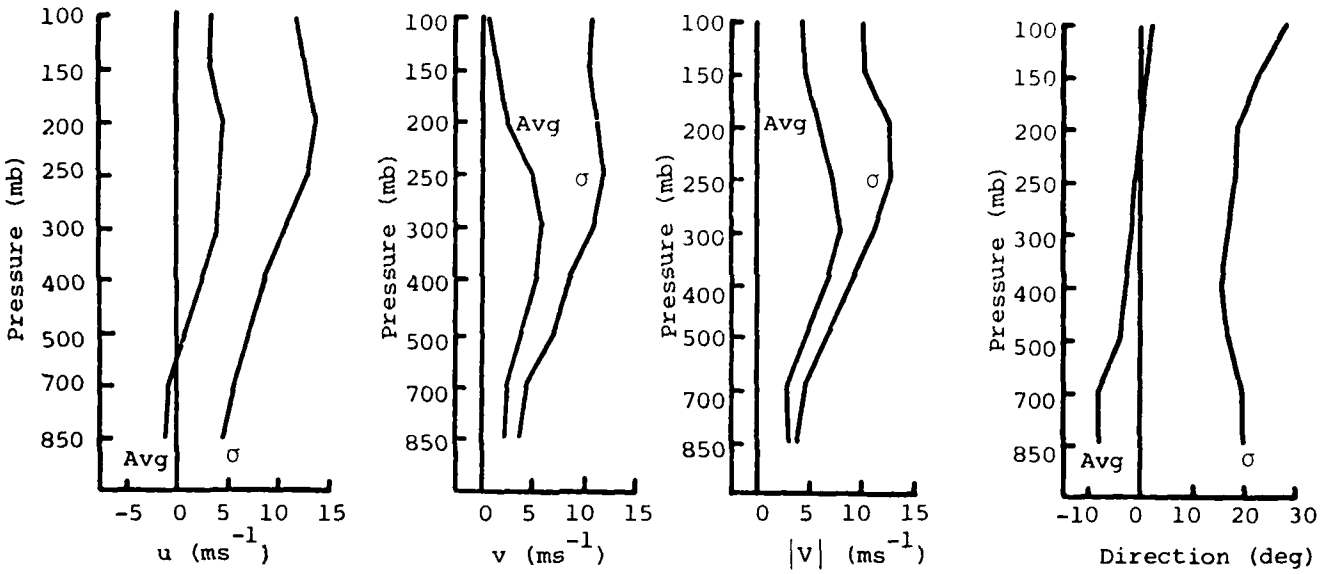

Fig. 32. Profiles of average and standard deviation of differences between geostrophic winds computed from rawinsonde and satellite geopotential heights for the AVE-SESAME area. Differences were computed by subtracting rawinsonde from satellite values.

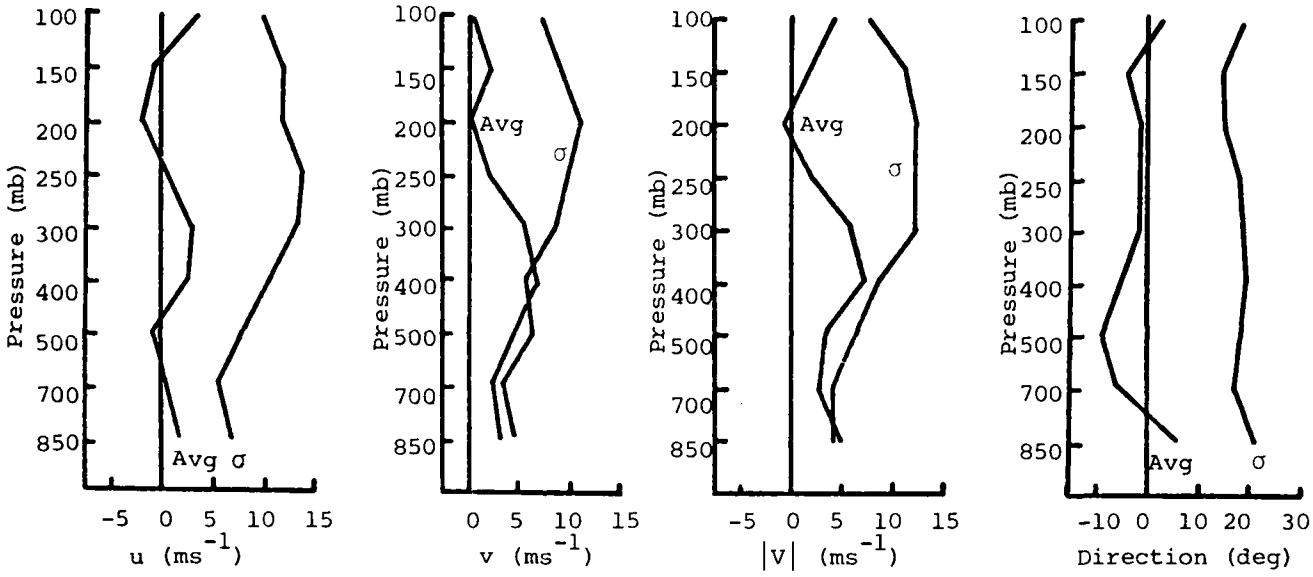

Fig. 33. Profiles of average and standard deviation of differences between rawinsonde winds and satellite-derived geostrophic winds for the AVE-SESAME area. Differences were computed by subtracting rawinsonde from satellite values.

wind speed are positive at most levels which indicates that satellite-derived geostrophic wind speeds are larger, on the average, than rawinsonde wind speeds. The standard deviation of the differences in scalar wind speed increases from about 4 m s^{-1} at 850 mb to approximately 12 m s^{-1} between 300 and 200 mb, then decreases to near 7.5 m s^{-1} at 100 mb. Average differences in wind direction range from about -10 to 10°, while the standard deviation is relatively constant at about 18°. Results obtained for the present area for wind speed are similar to those in the first United States area. Differences in wind direction are significantly smaller in the AVE-SESAME area.

8. SUMMARY AND CONCLUSIONS

8.1 Summary

The capabilities of Nimbus-6 and TIROS-N satellite sounding data for use in determining atmospheric structure have been investigated for several geographic areas. An evaluation of the ability of the satellite data to depict structural features of the atmosphere was based on comparisons between satellite and rawinsonde data. Nimbus-6 data were compared to time-interpolated rawinsonde data, and simultaneous TIROS-N and rawinsonde data were compared. Two approaches to the analysis and comparison of satellite and rawinsonde data were followed: 1) differences between paired soundings of satellite and rawinsonde data were computed, and 2) data from the satellite and rawinsonde soundings for selected constant-pressure surfaces were gridded and values from the two sets of data were compared at the grid points.

8.2 Conclusions

The following conclusions were reached from the results of this research:

(1) The approximate mean RMS of the discrepancies for profile pairs between Nimbus-6 and time-interpolated rawinsonde data for seven parameters and all seven areas are the following:

(a) Temperature: 2°C

(b) Dew-point temperature: 7.5°C

(c) Layer thickness: 7 m km^{-1}

(d) Mixing ratio: 1.34 g kg^{-1}

(e) Precipitable water: 0.23 cm

(f) Lapse rate of temperature: 1.1°C km^{-1}

(g) All Showalter indexes derived from satellite data are positive, and the vertical totals index is within 5% of and smaller than those computed from rawinsonde data.

(2) Cumulative frequency distributions show that discrepancies between Nimbus-6 and rawinsonde data can be represented by a normal distribution.

(3) For temperature and temperature-related variables, there is a strong correspondence between gridded fields of rawinsonde and Nimbus-6 data. Temperature differences are significant only in regions of strong vertical or horizontal gradients. In cross sections and constant-pressure

charts, the satellite data yield similar patterns to rawinsonde data, except that frontal contrasts are somewhat smoothed so that gradients behind fronts are not quite as strong in the satellite data. Differences between satellite and rawinsonde temperatures tend to be largest near the tropopause and the ground. Lapse rate of temperature, along with temperature, is useful for determining frontal locations from satellite data.

(4) For gridded fields of dew-point temperature and other measurements of moisture, the Nimbus-6 soundings present a smoothed version of rawinsonde soundings. Examination of dew-point temperature itself seems to yield poor results in terms of the depiction of frontal contrasts and in terms of quantitative differences between satellite and rawinsonde values. Equivalent potential temperature, which combines temperature and moisture measurements, is shown to be a better variable for depicting frontal locations.

(5) Differences between rawinsonde and satellite-derived fields of geopotential height tend to increase toward the tropopause and decrease slightly above that level.

(6) Results indicate that the best satellite-derived wind on constant-pressure charts is a geostrophic wind derived from highly smoothed fields of geopotential height. Satellite-derived winds computed in this manner and rawinsonde winds show similar circulation patterns except in areas of small height gradients. Magnitudes of the standard deviation of the differences between satellite-derived and rawinsonde wind speeds range from about 3 to 12 m s^{-1} on constant-pressure charts and peak at the jet-stream level.

(7) Fields of satellite-derived surface wind computed with the logarithmic wind law agree well with fields of observed surface wind in most regions. Magnitudes of the standard deviation of the differences in surface wind speed range from about 2 to 4 m s^{-1}, and satellite-derived surface winds are able to depict flow across a cold front and around a low-pressure center.

(8) Results obtained from the comparison of simultaneous TIROS-N and rawinsonde data are similar to those found for Nimbus-6 and time-interpolated data. The only significant change in the results was that found for the differences between satellite-derived and rawinsonde wind direction.

Magnitudes of the average and standard deviation of the differences between TIROS-N and rawinsonde wind directions are approximately half as large as the corresponding differences for Nimbus-6 and rawinsonde data. The improved results for wind direction with TIROS-N data may be due to the synoptic conditions in the area or the use of simultaneous rawinsonde and satellite data.

REFERENCES

Arnold, J. E., J. R. Scoggins, and H. E. Fuelberg, 1976: A comparison between Nimbus-5 THIR and ITPR temperatures and derived winds with rawinsonde data obtained in the AVE II experiment. NASA Contractor Report CR-2757, 76 pp.

Barnes, S. L., 1964: A technique for maximizing detail in numerical weather map analysis. J. Appl. Meteor., 3, 396-409.

Fiedler, F., and H. A. Panofsky, 1972: The geostrophic drag coefficient and the effective roughness length. Quart. J. Roy. Meteor. Soc., 98, 213-220.

Garratt, J. R., 1977: Review of drag coefficients over oceans and continents. Mon. Wea. Rev., 105, 915-929.

Grody, N. C., C. M. Hayden, and W. C. Shen, 1979: Typhoon June Winds Estimated From Scanning Microwave Spectrometer Measurements at 55.45 GHz. J. Geophys. Res., 84, 3689-3695.

Hanel, R., and B. J. Conrath, 1969: Interferometer experiment on Nimbus 3: Preliminary Results. Science, 165, 1258-1260.

Hilger, D. W., and T. H. Von der Haar, 1977: Deriving mesoscale temperature and moisture fields from satellite radiance measurements over the United States. J. Appl. Meteor., 16, 715-726.

Horn, L. H., R. A. Pedersen, and T. M. Whittaker, 1976: Intercomparisons of data derived from Nimbus 5 temperature profiles, rawinsonde observations and initialized LFM model fields. Mon. Wea. Rev., 104, 1363-1371.

Kapela, A. F., and L. H. Horn, 1975: Nimbus-5 satellite soundings in a strongly baroclinic region. Meteorological Applications of Satellite Indirect Soundings, Project Report, NOAA Grant 04-4-158-2, Department of Meteorology, University of Wisconsin, Madison, 1-19.

Petersen, R. A., and L. H. Horn, 1977: An evaluation of 500-mb height and geostrophic wind fields derived from Nimbus-6 soundings. Bull. Am. Meteorol. Soc., 58, 1195-1201.

Shuman, F. G., 1957: Numerical methods in weather prediction: II Smoothing and filtering. Mon. Wea. Rev., 85, 357-361.

Smith, W. L., H. M. Woolf, C. M. Hayden, and W. C. Shen, 1975: Nimbus-5 sounding data processing system part II: Results. Final Report, NASA Contract S-70249-A6, 35 pp.

Staelin, D. H., A. H. Barrett, and J. W. Waters, 1973: Microwave Spectrometer on the Nimbus 5 satellite: Meteorological and Geophysical data. Science, 182, 1339.

Wark, D. Q., and D. T. Hilleary, 1969: Atmospheric temperature: Successful test of remote probing. Science, 165, 1256-1258.

Waters, J. W., K. F. Kunzi, R. L. Pettyjohn, R. K. L. Poon, and D. H. Staelin, 1975: Remote sensing of atmospheric temperature profiles with the Nimbus 5 microwave spectrometer. J. Atmos. Sci., 32, 1953-1969.

Wilcox, R. M., and F. Sanders, 1976: Comparison of layer thickness as observed by Nimbus E microwave spectrometer and by radiosonde. J. Appl. Meteor., 15, 956-961.

1 REPORT NO.	2. GOVERNMENT ACCESSION NO.	3. RECIPIENT'S CATALOG NO.
NASA RP-1070	AD-A074272	

4. TITLE AND SUBTITLE	5. REPORT DATE
A Comparative Analysis of Rawinsonde and Nimbus 6 and Tiros N Satellite Profile Data	January 1981
	6. PERFORMING ORGANIZATION CODE
7. AUTHOR(S) James E. Scoggins, William E. Carle, Keith Knight, Vance Moyer, and Nine-Min Cheng	8. PERFORMING ORGANIZATION REPORT #
9. PERFORMING ORGANIZATION NAME AND ADDRESS Department of Meteorology Texas A&M University College Station, Texas 77843	10. WORK UNIT NO. M-327
	11. CONTRACT OR GRANT NO.
12. SPONSORING AGENCY NAME AND ADDRESS U.S. Army Research Office Research Triangle Park, North Carolina	13. TYPE OF REPORT & PERIOD COVERED Reference Publication
	14. SPONSORING AGENCY CODE

15. SUPPLEMENTARY NOTES

The U. S. Army Research Office has granted permission for NASA to publish these data for use in studies using space technology for weather-related programs.

16. ABSTRACT

This report addresses the question regarding the extent to which satellite sounding data can be used to determine atmospheric structure. Comparisons are made between rawinsonde and satellite profiles in seven areas for a wide range of surface and weather conditions. Variables considered consist of temperature, dewpoint temperature, thickness, precipitable water, lapse rate of temperature, stability, geopotential height, mixing ratio, wind direction, wind speed, and kinematic parameters, including vorticity and the advection of vorticity and temperature. In addition, comparisons are made in the form of cross sections and synoptic fields for selected variables.

Sounding data from the NIMBUS-6 and TIROS-N satellites were used. The NIMBUS-6 data were linearly interpolated to obtain soundings coincident in time with the rawinsonde soundings. The TIROS-N data were obtained concurrently with the rawinsonde data, and no interpolation was performed. Results from the analysis of the discrepancies between satellite and rawinsonde data were similar for both types of satellite data. Biases were observed in both sets of satellite data as a function of altitude, and the discrepancies were approximately randomly distributed in the 1000-500, 500-300, and 300-100 mb layers.

Geostrophic wind computed from smoothed geopotential heights provided large-scale flow patterns that agreed well with the rawinsonde wind fields. Surface wind patterns as well as magnitudes computed by use of the log law to extrapolate wind to a heighth of 10 m agreed well with observations.

The results of this study demonstrate rather conclusively that satellite profile data can be used to determine characteristics of large-scale systems but that small-scale features, such as frontal zones, cannot yet be resolved.

17. KEY WORDS	18. DISTRIBUTION STATEMENT
Meteorological satellite data Satellite-derived soundings Satellite-derived winds AVE-SESAME data	Unclassified - Unlimited Subject Category 47

19. SECURITY CLASSIF. (of this report)	20. SECURITY CLASSIF. (of this page)	21. NO. OF PAGES	22. PRICE
Unclassified	Unclassified	83	A05

For sale by National Technical Information Service, Springfield, Virginia 22161

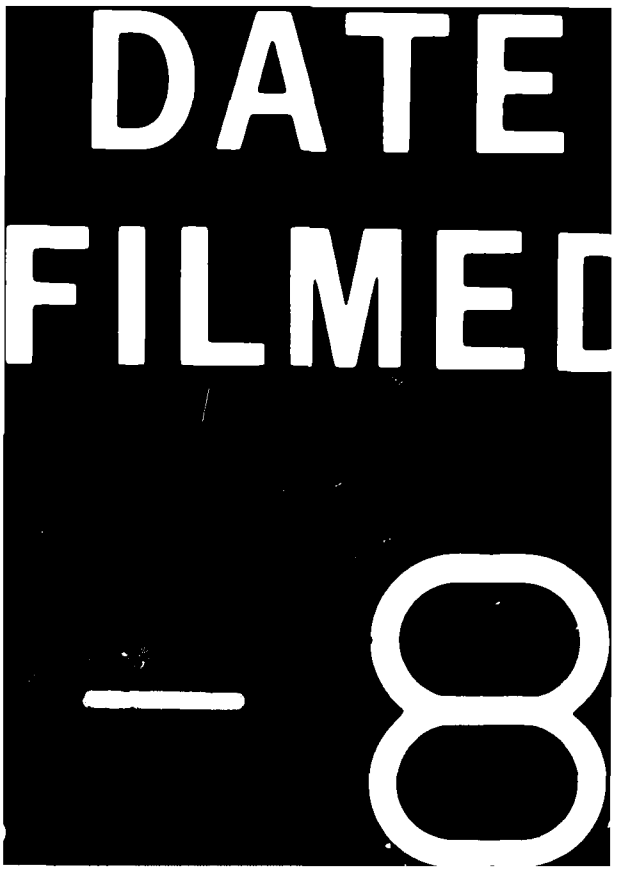
DATE
FILMED
8